10716
NACA TN 4372

TECH LIBRARY KAFB, NM
0067144

NATIONAL ADVISORY COMMITTEE FOR AERONAUTICS

TECHNICAL NOTE 4372

EFFECT OF PRECIPITATE PARTICLES ON CREEP OF ALUMINUM-COPPER ALLOYS DURING AGE HARDENING

By E. E. Underwood, L. L. Marsh,
and G. K. Manning

Battelle Memorial Institute

Washington
September 1958

AFMDC
TECHNICAL LIBRARY
AFL 2

TECH LIBRARY KAFB, NM

0067144

X

NATIONAL ADVISORY COMMITTEE FOR AERONAUTICS

TECHNICAL NOTE 4372

EFFECT OF PRECIPITATE PARTICLES ON CREEP OF ALUMINUM-COPPER ALLOYS DURING AGE HARDENING

By E. E. Underwood, L. L. Marsh,
and G. K. Manning

SUMMARY

Spherical or platelike precipitates were prepared in aluminum alloys with 1 to 4 weight percent copper. The effects of controlled sizes and distributions of particles were determined by creep, tensile, and hardness measurements, by quantitative metallographic evaluation of the particle characteristics, and by X-ray and electron-microscope examinations.

Single-phase strength curves, interpolated between high-temperature and room-temperature data, give the strength of the alloy matrix which is then subtracted from the measured strength of the particulate alloy. The difference is thus a measure of the contribution of the particles to the strength of the alloy.

For spherical particles the usual decrease in strength with increasing spacing is noted up to a critical spacing of about 50 microns. Beyond this critical spacing the strengthening due to spherical particles increases to a large value at spacings of about 500 microns. The same shape of curve is obtained from room-temperature tensile strengths as with minimum creep rates, in spite of the profuse stress-induced precipitation that occurs during the creep tests.

Platelike particles, on the other hand, show increased strengthening as the spacings increase to about 15 microns, then a decrease in strengthening follows with wider spacings. At room temperature the particle strengthening of platelets reaches about double the highest value attained by spherical particles.

Reversals in the overall strengths of alloys with fine or coarse spacings (less than the critical) are noted. At low and high stresses alloys with finer spacings are stronger than those with coarse; at intermediate stresses the alloys with coarse spacings are stronger.

The importance of the matrix composition in relation to alloy strength is shown. Precipitation during the test does not necessarily increase the strength of a two-phase alloy above that of a single-phase alloy with the same overall composition.

INTRODUCTION

The plastic properties of alloys with hard particles dispersed in a softer phase are generally believed to depend on the mean distance between the particles. However, as more detailed investigations are made, more discrepancies in the original simple relationships become apparent. As the limits of particle spacings and sizes are broadened, as the temperature of the test is extended upward, and as the time of test is lengthened, additional data conflicting with the early views and theories are uncovered.

The importance of particulate alloys, from the standpoint of increased performance at elevated temperatures and under increased loads, makes further detailed studies of particle strengthening effects particularly worthwhile. Modern advances in experimental techniques, especially in quantitative metallography, have pointed up the possibility of profitably undertaking additional work in this field. The analysis of the behavior of alloys with very fine particles is also more promising since the increased availability of the electron microscope augurs a new and rewarding treatment of small-particle effects. Recent improvements in quantitative mathematical methods for obtaining the size distribution curves for three-dimensional particles, from measurements made on the two-dimensional plane of polish, should also lead to important findings.

The complex nature of commercial creep-resistant alloys usually prevents an evaluation of the basic factors that contribute to their desirable qualities. By simplifying the experimental conditions, the basic factors may be uncovered more readily. This policy has been pursued here by investigating the effects of relatively controlled precipitate shapes, sizes, amounts, and distributions on the strength of high-purity alloys of aluminum-copper. By appropriate heat treatment procedures particles approaching true spheres have been obtained; likewise, alloys with remarkably large platelike particles were made available for study. With the somewhat artificial conditions obtainable in the laboratory, alloys have been produced with particle spacings much larger than those previously available for study. Thus, it has been possible to delineate behavior patterns that have not been detected previously and which may lead to a more general, rational explanation of observed effects in commercial alloys.

This investigation was conducted at Batelle Memorial Institute under the sponsorship and with the financial assistance of the National Advisory Committee for Aeronautics. The authors wish to acknowledge the assistance of Mr. R. D. Smith throughout the experimental program and the services of Messrs. John Roach, James Shambach, Lester Giesel, and Harold Hawkins. Photomicrographs were prepared under the supervision of Mr. Robert Buchheit; electron-microscope pictures were prepared by Mr. Arthur Young, and the X-ray results, by Mr. John Schroeder.

SYMBOLS

A	area
$\bar{A}$	mean surface area of particles
a,b,c	constants
d	atomic spacing
f	volume fraction of precipitate
G	shear modulus
K	mechanical properties
L	length
N	number of dislocation loops around each particle
N_L	number of particles per unit length along random lines
N_A	number of particles per unit area
N_V	number of particles per unit volume
n	number of particles of certain size
R	radius of circular trace of particles intersected by slip plane
r	radius of spherical particles
$\dot{S}$	mean spacing from particle center to center, $1/N_L$
V	volume
λ	mean free path
σ_y	yield stress
τ_h	hardening increment of back stresses

Subscripts:

i	size subdivision
p	particle
t	total

BACKGROUND

Many examples of the effects of dispersions on the strength properties of alloys are available in the literature. The overall problem has been reviewed recently (ref. 1) with a distinction being drawn between alloys composed of ductile phases and those containing hard intermetallic phases dispersed in a relatively soft ductile matrix. The present investigation is concerned with alloys belonging to the latter classification.

Early investigations of the effect of the microstructure of alloys on their strength were qualitative in nature and dealt mostly with room-temperature mechanical properties. Later, because of an increasing interest in high-temperature applications, more attention was paid to creep and creep-rupture testing. Qualitative studies of the relative high-temperature performance of alloys were based on the initial microstructure, on the initial grain size, or on different heat treatments.

Unfortunately, conflicting results were obtained which could not be resolved readily on the basis of the available information. For example, in some cases a larger grain size resulted in an increased creep strength, whereas the opposite behavior was noted in other instances. Also, the microstructure yielding the maximum creep resistance under one set of conditions was not necessarily the best structure for another temperature or stress. Similarly, a more disperse particle distribution was frequently associated with increased strength, yet the opposite behavior was often noted under other conditions.

Gensamer and his co-workers (ref. 2), in 1942, were among the first to realize the benefits of a quantitative study of the strength of particulate alloys. Their analysis of the tensile strength of steels heat-treated to various microstructures showed that the strength decreased linearly as the logarithm of the mean free path between the particles increased, regardless of the specific shape or amounts of the particles. Roberts, Carruthers, and Averbach (ref. 3) confirmed the essential aspects of Gensamer's findings. Later, Shaw and co-workers (ref. 4) reported that a better correlation existed for overaged aluminum-copper

alloys when the logarithm of the strength was plotted against the logarithm of the mean free path. Furthermore, they too concluded that the strength did not depend on the amount of the dispersed phase.

The latter conclusion conflicted with other published results on tempered carbon steels. Shimura and Esser (ref. 5) correlated the hardness of tempered steels with the number of carbide particles per unit area. They found that, contrary to the results previously quoted, a family of smooth curves resulted for the different carbon compositions. Hyam and Nutting (ref. 6) plotted the particle spacing of carbides in tempered steels versus the hardness at room temperature and also found a compositional dependence on the carbon content. They used the electron microscope to extend the resolution to particles less than a micron in diameter. It is remarkable that they obtained no agreement with any existing theory of particle hardening. The differences between their results and those of previous investigators were attributed to the finer range of particles covered by them, where the effect of volume fraction of precipitate is more marked. They did express the belief that substantial confirmation of Gensamer's linear relationship was obtained, but sharp breaks in some of their curves make this conclusion hard to accept.

The tensile properties of particulate alloys have been reported recently in some detail in a series of papers. Keeler (ref. 7) tested zirconium-chromium alloys at temperatures between -195° and 500° C. He concluded that a linear relationship existed between the flow stress and the volume fraction of zirconium dichloride, even though slight additional strengthening effects were noted in those alloys with more numerous, finer particles. The volume fraction of precipitate was calculated from the phase diagram and the assumed densities of the phases. The data did not clearly distinguish between the theoretical predictions of particle hardening advanced by Orowan (ref. 8) or by Fisher, Hart, and Pry (ref. 9). Hibbard and Hart (ref. 10) showed that the increment in flow stress due to the precipitate in copper-chromium alloys increased with the volume fraction of the dispersed phase. This increase was not linear, however, contrary to Keeler's findings. Agreement with the theoretical predictions of Fisher, Hart, and Pry was obtained by Reiter and Hibbard (ref. 11) working with iron-molybdenum alloys, and also by Hibbard and Hart, with copper-chromium alloys. In both of these investigations the volume fraction of the precipitate was calculated.

A comprehensive coverage of particulate aluminum-copper-alloy behavior was undertaken by Giedt, Sherby, and Dorn (ref. 12) by means of tensile and creep tests at elevated temperatures. The strengths of two 3-percent-copper alloys, one with a fine particle spacing and a fine grain size and the other with a coarse dispersion and a large grain size, were compared on the basis of their initial (calculated) mean free paths.

They found that the alloy with the finer spacing gave higher strengths at lower and higher stresses, while the coarser spacings resulted in higher strengths at intermediate stresses. How much of this reversal in relative strengths is due to changes occurring during the test is problematical, but data from both the short-time tensile and longer creep test were correlated on the same curves.

Since Dorn's work stands alone, it may be well to discuss a few other aspects of this investigation. The usual straight-line relationship was found when the logarithm of the creep stress was plotted against the logarithm of the minimum creep rate but only at the lower temperatures of 77° to 204° C. At higher temperatures, from 257° to 305° C, unpredictable curves were obtained. This is explicable on the basis that grain growth and stress-induced precipitation occurred during the course of the creep test, but apparently the microstructures were not examined afterwards. It is particularly unfortunate that the two dispersion alloys selected for the detailed examination did not have the same initial grain size. This would have been desirable in order to delineate more clearly the effects due to the particle dispersions.

The proceding detailed comments have been offered in order to emphasize the need for further work in this important field. It is evident in this brief review of the few cases where quantitative studies have been attempted that the amount of precipitate has usually been calculated. There is now a reasonable basis for suspecting the accuracy of this method when small particles are involved. In two cases, reported by Underwood, Marsh, and Manning (ref. 13) and by Hyam and Nutting (ref. 6), the volume fraction of the particles was obtained by actual quantitative measurements. In both cases, an anomalously large amount of precipitate was found above that predicted by the phase diagram. Qualitative confirmation of this effect has been found in the literature. Therefore, it is felt that in any investigation concerned with small particle effects the amounts of precipitate should be measured directly, if at all possible.

A point which warrants closer attention is the effect of changes in the concentration of the matrix of alloys tested at different temperatures. In order to evaluate accurately the particle-strengthening increment ΔS of the alloy, it is necessary to subtract the contribution to strength of the solid solution. The resulting ΔS then reveals the increase in strength ascribable to the presence of the particles.

In addition to these experimental studies, a number of theoretical analyses have been advanced. They are based largely on dislocation theory of plastic flow and require the use of several simplifying assumptions. The assumptions made are that the particles are (1) spherical, (2) uniform in size, (3) randomly dispersed in the matrix, and (4) do not deform with the matrix. It is evident that all these conditions are seldom, if ever, encountered in practice.

Orowan (ref. 8) extended the theory of precipitation hardening put forward by Mott and Nabarro (ref. 14) to include the case of coarse, overaged precipitates. A dislocation line, held up by a pair of particles of spacing λ, was imagined to bulge between the particles under an applied stress until loops of radius $\lambda/2$ were formed at the yield stress σ_y. His expression, in the notation of the present paper,

$$\sigma_y = \frac{2Gd}{\lambda} \tag{1}$$

where G is the shear modulus and d is the atomic spacing, predicts that the strength of an alloy should be proportional to the reciprocal of the spacing. It will be recalled that Gensamer found that the strength varied inversely with the logarithm of the mean free path. In reference 4 the authors applied the concepts of both Gensamer and Orowan to their data but concluded that the logarithm of the mean free path correlated better with the logarithm of the flow stress.

A different hardening mechanism, proposed by Fisher, Hart, and Pry in reference 9, was based on another dislocation model. Particles intersecting the slip plane are surrounded by many small closed dislocation loops. The loops set up back stresses which raise the effective critical stress of all Frank-Read sources in the plane. The hardening increment identified with these back stresses is given by

$$\tau_h = 3f^{3/2}\,\frac{N}{R} \tag{2}$$

where R is the radius of the circular trace of the particles intersected by the slip plane; N is the number of dislocation loops around each particle; f is the volume fraction of the precipitate, and τ_h is the hardening increment, or the difference in stress for equal strain of the two-phase structure and the single-phase matrix. Their expression predicts that the hardening increment should vary inversely with the particle radius. Some agreement with experiment was claimed, although the scatter was considerable.

An expression relating mechanical properties K to the distance λ between particles (or phases) was derived by Unckel (ref. 15), who considered the shearing forces acting in successive layers below the plane of application of the deforming stresses. His equation,

$$K = ae^{-b\lambda} + c \tag{3}$$

where a, b, and c are constants, appears to have general application not only to his diverse data but also to the data of other investigators (refs. 2, 3, and 4). It was found, as shown by Westbrook in reference 4, that Unckel's function provided a better fit to the experimental data than did the expressions suggested by the authors of references 2, 3, and 4. Furthermore, his formulation has the merit that, at zero spacing, the deformation strength of the second phase is given by a plus c, and at infinite spacing the deformation strength of the matrix is equal to c.

The experimental investigations and theoretical treatments are laudable attempts at clarification of the problem of particle hardening. However, the generality of the results is necessarily limited by the assumptions introduced. Also, it is necessary to restrict the experimental scope in order to reduce the large number of variables involved. Westbrook has classified all the pertinent variables into two categories:

(1) The microstructural factors: the amount, size, shape, and distribution of the second phase

(2) The physical factors, or the properties of the matrix and embedded phase: the ductility, strength, work-hardening capacity, crystallographic misfit, interfacial energy, and interfacial bond strength

Because of the multiplicity of variables involved, it is necessary to investigate only a few of the most significant factors and to attempt to hold the others reasonably constant. It is believed that the microstructural factors are the more important because, in almost every case, the strength correlations have been obtained with either the amount, size, or spacing of the particles. These correlations may be taken as evidence that interfacial energy, interfacial bond strength, and so forth, are relatively unimportant in alloys with incoherent particles.

EQUIPMENT AND EXPERIMENTAL PROCEDURES

Specimens

Four alloys of 1, 2, 3, and 4 weight percent copper were prepared from 99.996 percent aluminum and 99.999 percent copper. The details of melting and fabrication have been recorded in a previous report, reference 13. Spectrographic and chemical analyses are listed in table I for the four sections of each ingot.

The bulk of the creep and tensile testing was performed on flat tensile specimens $2\frac{11}{16}$ inches long, $\frac{9}{16}$ inch wide at the shoulders, and $\frac{1}{8}$ inch thick. The gage sections were 0.250 inch wide and 1 inch long.

Other tests utilized a 7-inch flat tensile specimen or a flat tandem specimen $7\frac{3}{4}$ inches long.

After heat treatment to an ASTM grain size of 0 ± 1, the specimens were electropolished in a glacial acetic acid and perchloric acid solution. Knoop indenter impressions were placed 1 inch apart on the gage section of the short specimens and were used as gage marks during the creep runs.

Creep Measurements

The creep equipment was housed in a constant-temperature room at 26° ± 1° C. The furnace temperatures could be controlled within ±2° C, and the temperature variation along the specimen was held to within ±1/2° C.

Direct loading was utilized for the constant-load creep runs, and the applied load was determined within 0.1 pound. The creep elongation was measured optically, from outside the furnace, with a sensitivity of about 50 microinches. The pertinent creep data are presented in table II.

Tensile and Hardness Measurements

Room- and elevated-temperature tensile tests were run at a constant strain rate of 3.18 percent per minute. The specimens were held by yoke and pin adaptors and gripped at the shoulders, and the load was applied through a 9:1 lever arm. The stress was determined from a calibrated ring gage and the strain was read from a dial gage, which could be read to 0.0001 inch, attached to the upper extension arm. The tests were usually discontinued shortly after the maximum load was detected.

Room-temperature hardnesses were obtained from the tensile-tested specimens, as well as from untested samples prepared for the metallographic work. A Vickers hardness tester was used with a 10-kilogram load, and the average of at least four impressions was taken. Tensile and hardness data are recorded in table III.

X-Ray Methods and Electron Microscopy

An X-ray diffraction examination was performed on samples heat-treated to the desired conditions. Since the grain size was quite large it was necessary to resort to filings. However, in order to preserve the actual conditions of the alloys, the filings could not be annealed prior to the X-ray exposure. Thus, some line broadening due to strain could not be avoided. The accuracy was estimated to be within ±0.001 angstrom unit. The X-ray data are summarized in table IV.

Other tests were made from the surface of the metallographically mounted samples with an RDX-3 spectrometer made by the General Electric Co. In these cases sharp peaks were obtained giving agreement with the results from the filings within the limit of experimental accuracy (±0.0006 angstrom unit). Figure 1 gives an idea of the unusual X-ray data obtained under these conditions. Alloys were given the indicated heat treatments, then were analyzed spectrographically, and subjected to both types of X-ray measurements mentioned above. No matrix compositions should fall above the solid line, and the overaged alloy values should conform closely to the dashed line. These data are discussed later, and some justification of the anomalous results is offered. Selected samples were also photographed at magnifications of X6,000 or X18,000 by means of the electron microscope from shadowed silicon replicas obtained from a plastic impression.

Quantitative Metallography

Four main types of quantitative measurements were made on representative alloys:

(1) A lineal analysis was made by the method described in reference 16. A microscope, Hurlbut counter, and movable microscope stage gave volume fraction of the second phase.

(2) A method of analysis described by Scheil in reference 17 was used. The areas of spherical particles were traced from their images projected on the screen of a Bausch and Lomb metallograph. The areas were then measured with a planimeter, and a modified version of the analysis by Schwartz (ref. 18) was applied to the two-dimensional data.

(3) A chord-intercept method described by Lord and Willis in reference 19 was used. A random straight line along the plane of polish was intercepted by the circular traces of the spherical particles. The chord lengths were measured individually by means of the Hurlbut counter.

(4) The lengths and thicknesses of platelike precipitates were obtained from photomicrographs at a magnification of X1,500. Individual measurements of the thickness of each fine platelet were not warranted at this magnification; therefore an average thickness was determined and assigned to all platelets in each photomicrograph. However, the length of each platelet was recorded individually. The method outlined by Fullman in reference 20 was used to analyze the data.

The volume fraction of spherical precipitate was measured primarily by means of lineal analysis; however, the Scheil and the Lord and Willis analyses also yielded the same information. The results from these three methods agreed closely with a maximum deviation of about 0.2 volume percent.

The mean particle size (or radius) was determined from the Scheil or Lord and Willis analyses, or from the equations of Fullman. The volumetric mean free path and the mean planar particle spacing (center to center) were calculated from area or lineal particle-density counts and were determined over a wide range of values. Quantitative particle data are summarized in table V.

EXPERIMENTAL RESULTS AND EVALUATION

The problem of obtaining the desired types and amounts of precipitate particles was attacked from two directions. In one case spherical particles were first developed by overaging, then partially redissolved in the single-phase field for various times in order to produce lesser amounts of spherical particles. In the other case a platelike precipitate was developed from single-phase alloys by aging at selected temperatures. These temperatures were determined by previous studies (ref. 13) to be those where the rate of age-hardening was a maximum.

Figure 2 depicts schematically the temperatures involved in heat treating each of the four alloys and also the solvus between the single- and two-phase regions and the temperatures where the alloys overage the fastest. At the latter temperatures less than 30 minutes are required to overage the four alloys; therefore the 3 days at temperature should result in alloys close to equilibrium.

The details of heat treatment are given in table VI. For the spherical particles listed for 4-percent-copper alloys, a short high-temperature anneal was given (1) before overaging (θ_I particles) or (2) after overaging (θ_{II} particles). The anneal in treatment (1) relieved strains due to prior cold-work and gave a large grain size before overaging. Treatment (2) brought the grain size to that desired and also rounded off the particles considerably. In addition, the amount of precipitate was diminished about 0.12 volume percent by the high-temperature anneal. Next, for both series of alloys the particles were progressively dissolved at a lower temperature within the single-phase field. In this way further grain growth was minimized and successively smaller size distributions of spherical particles were produced. Examples of the degree of sphericity attained by procedures (1) and (2) (table VI) are shown in the photomicrographs in figure 3. Note the unusually large particle spacings.

It should be noted that the preliminary soak at 540° C was essential in order to form platelets. If the cold-worked alloys were aged directly at their respective temperatures, the particles were largely spherical; whereas, if they were annealed first, removing the residual strains from

cold-working, the metastable platelike θ' particles could persist. Examples of θ' precipitates are shown in figure 4 for the 2-, 3-, and 4-percent-copper alloys.

The increment of hardening ascribable to the particles is considered to be the difference in strength of the particulate alloy and that of an alloy with the same composition as the accompanying matrix. By overaging the alloys at different temperatures, the matrix solid solutions will have different copper contents. Also, the matrix compositions will be different when the precipitate is partially dissolved. Thus, rather extreme experimental conditions are available for evaluation of the particle-hardening increment. X-ray lattice parameter measurements give the effective copper content of the matrix, and the strength of this single phase can be calculated for the same conditions of temperature and stress as those under which the actual alloy was tested. Obviously, for temperatures and compositions that fall within the two-phase region, the strength of a single-phase alloy cannot be measured. However, the strengths of single-phase alloys can be measured at temperatures above the solvus and at room temperature, so the single-phase data can be interpolated between low and high temperatures. The reliability of this interpolation is aided considerably by the fact that the complete strength-temperature curve can be obtained experimentally for pure aluminum. Furthermore, references 21 to 25 indicate that the strength-temperature curves of nearly all materials have qualitatively the same general shape.

This point has been discussed in some detail because of the importance of these curves in calculating the strengthening increment due to particles. One further point should be recalled at this time. Since the strength properties under consideration here include both tensile and creep data (e.g., the minimum creep rate), it is advisable to incorporate both types of data in the single-phase curves. This is accomplished readily by plotting the strength data against a temperature—strain-rate parameter, such as the Larson-Miller parameter (ref. 26) or Z parameter as used by Sherby and Dorn (ref. 27), instead of against temperature alone.

Figure 5 presents the plot of strength (creep stress or ultimate tensile strength) versus a temperature—strain-rate parameter for aluminum and the four aluminum-copper alloys. Data from references 21, 28, 29, and 30 have been incorporated into this diagram to augment the data obtained in this investigation. The curve for pure aluminum is particularly well documented, both by tensile and creep data.

Much of the experimental creep testing was performed at a stress of 2,400 psi and a temperature of 300° C, and the minimum creep rates were calculated for hypothetical single-phase alloys under these conditions. The resulting curve appears in figure 6. The bump in the curve near 2 percent copper is apparently a real effect, and corresponds to a retardation in the rate of age-hardening that occurs near this temperature

and composition (see ref. 13). It will be noticed that the lowest minimum creep rate is plotted at the top of figure 6 and that the larger creep rates are at the bottom. In this way, the more creep resistant the alloy, the higher it appears on the plot. The room-temperature tensile-strength curve for single-phase alloys was calculated from figure 5 and is shown in figure 7, along with the experimentally determined points. The bump occurs in this curve also, but this is understandable if it is recalled that these alloys, although considered single phase at room temperature, are still thermodynamically unstable. Their room-temperature properties may be reflecting to some extent the influences that were operative at higher temperatures.

After the desired spherical and platelike precipitate particles were produced, it was necessary to evaluate their characteristics quantitatively. A knowledge of such characteristics as volume fraction, mean radius, mean free path, planar spacing, density of particles (lineal or area), and thickness-to-diameter ratio of the platelets is highly desirable.

Several methods are known whereby the volume fraction of a phase can be obtained from measurements on the two-dimensional plane of polish. Lineal analysis (ref. 16) is perhaps the best of these methods, since no assumptions are required of the particle size, shape, or distribution; the only requirements are that the phase be visible and distinguishable under the microscope and that a statistically sufficient coverage be obtained. By comparing the relative lengths of random lines intersected by the precipitate with the total length of the line, the volume fraction is obtained directly. The equality of lineal ratio, area ratio, and volume ratio is expressed by

$$\frac{L_p}{L_t} = \frac{A_p}{A_t} = \frac{V_p}{V_t} \tag{4}$$

where L, A, and V refer to length, area, and volume, respectively, and the subscripts p and t denote particle and total, respectively.

Other ways in which the volume fraction of precipitate can be obtained are by the Scheil (ref. 17) analysis, or by the method proposed by Lord and Willis (ref. 19). Both analyses permit the derivation of the three-dimensional particle characteristics from the trace of the particles on the two-dimensional plane of polish. The Scheil analysis utilizes a particle-area distribution curve, while the Lord and Willis method depends on the distribution curve of chord lengths intercepted by those particle traces which hit a random straight line. The assumptions required in these analyses are that the particles have spherical shapes and that a statistical coverage is obtained.

If a simple geometrical shape can be assumed for the particles, the volume fraction can be calculated easily from measurements of the appropriate dimensions of all particles (ref. 20). It is assumed that θ' platelets have the shape of a circular disk. Since it is very difficult to be completely certain that some slight etching effect has not disturbed the true thickness of these platelets, an average thickness was applied to all platelets in any one alloy. Thus, the volume fraction f is equal to

$$f = \sum N_{A_i} \bar{A}_i \tag{5}$$

where N_A is the number of particles per unit area and $\bar{A}$ is the mean surface area of the particles within a size subdivision i. The laboriousness of the measurements made it necessary to restrict the size of the sample; therefore the volume fractions should be considered only as relative values. Other results, such as the thickness-to-diameter ratios, should be fairly indicative of the actual platelet characteristics.

Both the volumetric mean free path and planar spacing were obtained in this investigation. The general relationship for the mean free path λ is given (refs. 6 and 20) as:

$$\lambda = \frac{1 - f}{N_L} \tag{6}$$

where f is the volume fraction of precipitate and N_L is the number of particles per unit length along random lines. This expression is valid regardless of the shape or distribution of sizes of the particles. The reciprocal of N_L is S, the mean spacing from particle center to center. For small particles S is much the same as the mean free path. It can be seen that, for small values of f, S is also practically equal to λ. The relative ease of measuring N_L makes S the preferred measure of interparticle distance.

The mean radius of spherical particles $\bar{r}$ can be calculated (ref. 31) by means of the expression:

$$\bar{r} = \frac{\sum r_i n_i}{\sum n_i} \tag{7}$$

where n_i is the number of particles of radius r_i and i designates the number of the subdivision into which the particles have been subdivided.

The surface density of particles N_A and the lineal density N_L were obtained by counting the number of particles on a given area from photographs and by counting the number of particles intersected by a random line across the microstructure, respectively. Since the number of particles which can be seen increases with the magnification, it is preferable to make comparisons involving particle densities with data obtained at the same magnification.

Spherical Particles

Table VI describes the three ways in which spherical particles were produced. For the spherical particles obtained at solvus temperature, the creep rate, tensile strength, and hardness values are compared as a function of solution time in figure 8. Again the logarithm of the creep rate has been plotted on a reversed scale, the higher the curve, the more creep resistant the alloys. The properties at the longer solution times, even up to 2 hours, do not appear to have reached their maximum values. Ultimately, however, the alloys should approach the single-phase condition and the strengths should decrease if the particles are responsible for the strengthening effects.

The creep resistance of the 1-percent-copper alloy decreases as solution time increases from 0 to 15 minutes, but the mean particle spacing also decreases, as shown in figure 9. This behavior is consistent with that found for the other alloys, in that as the measured strength values increase, so do the particle spacings. Thus, it appears that the stronger alloys are associated with the coarser spacings. However, it will be shown later that the increased strength obtained at longer solution times is due primarily to the enrichment of the matrix as the particles are dissolved.

The progressive improvement of the creep properties, as the over-aged alloys are given increasingly longer solution times, is seen in figure 10. For any one composition the time needed to reach a creep strain of 2 percent increases as the solution time increases (to 60 minutes). Data for single-phase alloys in which precipitation occurred during creep are included to emphasize the relative improvement of creep resistance in alloys with the higher initial matrix composition as compared with that of alloys with a more depleted matrix. In fact, calculated strengths of hypothetical single-phase alloys fall near the curve for the alloy given 60 minutes of solution treatment. This means that the measured strength of the particulate alloy is less, in spite of the strengthening effect of the particles, because of the lowered matrix strength.

It should be reemphasized that the particle spacing measurements were made before the creep test. Photomicrographs of the specimens taken after the creep test invariably showed profuse additional stress-induced precipitation throughout the alloy (see fig. 11). This point is all too frequently glossed over, or left unmentioned, in the literature. The fact that correlations can be made in terms of the initial microstructural characteristics reflects the marked persistence of the initial state on the subsequent alloy behavior. On the other hand, it may be that correlations between initial properties and the measured strength values are obtained only because the correct relative standings of the alloys are unchanged. In either case, the initial state appears to be a satisfactory criterion of alloy strength.

Lattice-parameter measurements of the matrix of alloys listed in table VI, under heat treatments of θ particles at solvus temperatures were obtained before creep-testing. The corresponding copper contents were calculated from the lattice-parameter data of Axon and Hume-Rothery (ref. 32). The percent copper in the matrix of these alloys is plotted versus the mean particle spacing of the alloy in figure 12(a). The double points at each spacing stem from the two types of X-ray measurements that were made, one from unannealed filings and the other from bulk specimens. The two distinct curves do not appear to be related too closely with one another and do not yield one continuous curve dependent on only the spacing.

The graph in figure 12(b) gives the measured minimum creep rate versus the mean particle spacing for a temperature of 300° C and a stress of 2,400 psi. Except for a few minor differences, the curves in figure 12(a) parallel those in figure 12(b) qualitatively. For the same particle spacing the overall strength of the alloy varies with the copper content of the matrix; therefore maximum strength should be attained near the limit of solubility. The efficacy of the matrix has been reported also in iron-base alloys (ref. 33) and may be the explanation of the increased strengths with solution time reported in reference 34. However, the possibility of particle size effects should not be ruled out. The abrupt increases in creep resistance which occur near the same spacings also involve a smaller mean particle size. The greater strengthening effects of small particles is in accord with the theoretical treatment advanced by Fisher, Hart, and Pry in reference 9.

The curves shown in figure 12(c) were obtained from figure 6 for single-phase alloys with the same composition as the matrix as revealed by X-ray measurements. If solid-solution strengthening is provided a major part of the strength in these alloys, the similarity of creep rate curves in figures 12(b) and 12(c) would not be entirely unexpected. In order to separate the effects due to particles, the difference between the curves in figures 12(b) and 12(c) must be taken. Further consideration of these data will be deferred until later when all the results for spherical particles will be presented.

An analysis similar to the preceding one can be made for the alloys with spherical particles given special heat treatments as indicated in Table VI. Relationships involving the volume percent precipitation and percent copper in the matrix are presented for these alloys in figure 13. The data in figure 13(a) were obtained by lineal analysis using the Hurlbut counter. Note the small amounts of precipitate involved. The slight rise preceding the final drop toward 0-percent precipitation has been shown by Hyam and Nutting (ref. 6) to be characteristic of larger particles. Smaller particles tend to dissolve immediately. Electron-microscope pictures of the θ_{II} alloys taken at X6,000 showed a progressive decrease in the number of smaller particles as the solution time increased. Since these smaller particles were still large enough to be seen at X1,000, they were not omitted from the particle density counts.

The matrix compositions shown in figure 13(b) vary inversely with the volume percent of precipitation, and this is shown directly in figure 13(c). The data point calculated from the phase diagram (2.6 volume percent) can be compared with the θ_I point at only zero solution time (0.95 volume percent). It appears that the deficiency of precipitate is related to the excess copper in the matrix. Regardless of whether the copper is in the matrix or in the precipitate, and regardless of the artificiality of the means employed to get these various combinations of precipitate amounts and matrix compositions, a linear relationship is obtained. The extensive data of Hyam and Nutting also reveal a linear relationship between $\log_e(N_v)$ and $\log_e(S)$. Such interrelationships reduce the number of variables needed to describe the behavior of particulate alloys and explain why the mean spacing S is so generally satisfactory as the primary variable.

Curves similar to those shown in figure 12 are reproduced for the θ_I and θ_{II} alloys in figure 14. Again the matrix compositions parallel the curves of measured and calculated minimum creep rates, and again no continuous curve is seen. If the difference in minimum creep rate between the alloy and its matrix is plotted versus particle spacing for all the alloys with spherical particles, the results shown in figure 15 are obtained. The tensile strength curve in figure 15(a) is to be thought of as the increase in strength due only to particles. It was obtained the same way that the creep curve in figure 15(b) was determined. Although there is considerable scatter in the data at the larger particle spacings, the trend is readily apparent. Much of the scatter stems from some erratic X-ray data, which indicated more copper in the matrix of the alloy than in the entire alloy. Use of these anomalous values is responsible for the negative increases in tensile strength. With more reasonable X-ray values, qualitatively the same type of curve would be obtained.

An alternate approach to this problem, which eliminates the anomalous X-ray data, is to calculate the matrix compositions of the overaged alloys from the phase diagram. The matrix composition of alloys given a 15-minute solution treatment can then be calculated by adding the change in copper content indicated by X-ray measurements to the equilibrium concentrations. This procedure yields more reasonable values of composition and insures that all the increases in tensile strength are positive. The results are summarized in figure 16. The data therein correspond to the tensile data of figure 15 between spacings of 0 and 0.2 millimeter. The dashed line represents the numerous data taken from reference 4, for 3-, 4-, and 5-percent-copper alloys. However, the calculated spacings given in reference 4 are seriously inconsistent and have been recalculated from the basic data. For spacings of about 0.05 millimeter (50 microns) and less, the usual increase in particle strengthening versus decreasing particle spacing is obtained. The unusual feature of this curve is that at spacings greater than about 50 microns, the particle strengthening increases with increased spacing to a large value near 500 microns (but finally must return to zero strength as the spacing becomes infinite).

The reason this effect has not been recognized more generally is probably due to the restricted range of spacings studied previously. The maximum spacings utilized by several investigators are indicated along the abscissa of figure 16 and generally did not exceed about 50 microns. It is apparent that the critical spacing for aluminum alloys has hardly been exceeded in these other investigations. This same critical limit may apply to steels, if the calculation by Westbrook (see ref. 4) of a critical spacing of about 50 microns is valid.

The curves of figures 15 and 16 also suggest that appreciable increases in particle strengthening can be obtained with alloys possessing a relatively coarse particle distribution. Although the increased creep resistance in alloys with an initial spacing greater than the critical might be attributed to the new, fine, stress-induced precipitate, no such explanation is available for the same alloys that were tensile-tested at room temperature. The similarity of the curves in figure 15 also points to a common basis for their strength behavior, and one that does not depend on precipitation. It may be that the initial particle distribution determines the strain patterns set up within the alloy when it is stressed and that the ensuing localized lattice fragmentation provides the main resistance to plastic deformation. Subsequent precipitation merely accommodates itself throughout the lattice and does not contribute significantly to the strength already established by the existing fragmentation pattern. These speculations have not been justified experimentally, yet the similarity of the tensile strength and creep resistance curves forces one to attach a greater degree of importance to the initial structure of the alloys than would be suspected.

Platelike Particles

The heat treatments given the alloys to obtain platelike particles of θ' are shown in table VI. A brief solution treatment before aging was found to be necessary for the formation of platelike particles. Examples of the microstructures are presented in figure 4 for alloys of 2, 3, and 4 percent copper. The precipitate in the 1-percent-copper alloys was unresolvable at X1,500 under the light microscope, but a dense array of dotlike precipitate, much like that shown by Wilsdorf and Kuhlmann-Wilsdorf in reference 35, was revealed by electron microscope pictures at a magnification of X18,000.

Room-temperature properties of the alloys after various times at their aging temperatures are portrayed in figure 17. As the aging time increases, the hardness, tensile strength, and particle spacing decreases. It is seen that the measured strength decreases with finer spacings. However, the matrix is being depleted of copper as precipitation proceeds, so it again appears that the decrease in matrix strength is not compensated for by the strengthening effects from the particles. Finite values of particle spacing are assigned the single-phase alloys at zero aging time since some particles or inclusions could be seen.

Erratic X-ray data were obtained from some of the specimens aged to produce a platelike precipitate. The copper content of the matrix is plotted as a function of aging time, as shown in figure 18(a). The curves should start from the overall composition of the alloy, then decrease to the equilibrium values indicated on the graph. Instead, unpredictable dips and rises precede the attainment of final equilibrium.

The minimum creep rates also exhibited unusual results as shown in figure 18(b). After 5-minute prior aging, and at low stresses, the creep resistance of the alloy decreased, then rose again after longer aging times. A decrease in creep resistance after aging in other alloys has been reported (ref. 36). Some parallelism seems to exist between the X-ray results and those from creep tests, although the dips in the minimum-creep-rate curves tend to flatten out at higher stresses.

Further justification for these unusual data may be deduced from known precipitation and dilatation measurements. The systematic decrease in the copper content of the matrix, at 5 minutes' aging time, with increasing alloy composition suggests a connection with the kinetics of the precipitation process. For the aging temperatures used here, the alloys with the greater copper content would react to a greater extent in the 5-minute period (ref. 13). Since a decrease in the copper content of the matrix corresponds to an increase in the amount of precipitate, an anomalously low matrix composition may be associated with the anomalously high amount of stress-induced precipitation reported in this system.

Furthermore, the dilatation measurements of Lankes and Wassermann in reference 37 for aging aluminum alloys containing 4 percent copper revealed an early, anomalous expansion which was attributed to the formation of the θ' phase. An increase in the lattice parameter corresponds, as shown by X-ray data, to a decrease in the copper content of the matrix or to the state of strain within the lattice, and may not be due entirely to a simple loss of copper atoms.

By the same token, the anomalously large increase in copper content of these alloys may be associated with a marked contraction of the lattice due to the type of precipitate evolved. For example, the precipitate in the 1-percent-copper alloys, as was seen in the electron-microscope pictures, consisted of finely dispersed, spherical particles.

With the available experimental results, the difference in minimum creep rates of the alloy and matrix were calculated as described before. The resulting increase in creep resistance is shown versus particle spacing in figure 19(a) for a test temperature of 200° C and a creep stress of 6,000 psi. Again, a recalculated spacing has been used with the data of Giedt, Sherby, and Dorn (ref. 12), and their point is included for purposes of comparison. Room-temperature tensile strengths were utilized to give the curve in figure 19(b), and a qualitative similarity to the curve in figure 19(a) is evident. This similarity of shape implies that the effect of the initial microstructure persists throughout the test and is essentially unaffected by precipitation during creep.

There are marked differences between these curves for alloys with platelike precipitate and those in figure 15 for alloys with spherical particles. The most striking difference, perhaps, is that the strength increase due to platelets increases with increasing particle spacing. This is contrary to the behavior observed for spherical particles. Furthermore, the critical spacing appears to be about 15 microns for the platelets. At room temperature the particle strengthening of platelets reaches about double the highest value obtained by spherical particles.

These differences may be considered from the standpoint of the type of particle involved or of the experimental conditions. A clue to the possible role played by the particle shape is afforded by the results of Giedt, Sherby, and Dorn. Data from their creep measurements (with the same alloy) are included in both figures 15 and 19, and are seen to agree with the creep data from this investigation. Thus, it may be concluded that particle shape does not determine the slope of the curve of particle strengthening versus spacing.

However, other findings by Giedt, Sherby, and Dorn, (embodied in their fig. 5) may be utilized to rationalize the results from all the creep data. The curves in their figure 5 indicate three regions, according to the stress involved, in which the relative strengths of

alloys with fine and coarse particle spacings are reversed. The three regions are indicated for alloys with spherical particles in the schematic drawing, figure 20. At high and low stresses the stronger alloys have finer spacings, while at intermediate stresses, alloys with coarser spacings have the higher creep stress.

It can now be recognized that the creep data in figure 15(b) and the creep data in figure 19(b) fall into the low- and intermediate-stress regions, respectively, with behavior appropriate to their location (see locations 1 and 2 in fig. 20). Of course, the agreement with the findings reported in reference 12, is valid only for particle spacings less than the critical. If a larger range of spacings were encompassed, it would be possible to obtain entirely different behavior.

The results from the tensile tests are more ambiguous than those for creep, because they do not fit in with the simple picture based on the curves for spheres in figure 20. The tensile data for the spherical particles appear to fall in the high-stress region, since the finer spacings yield higher strengths than the coarse. This would correspond to location 5 in figure 20. However, the tensile data for alloys with platelets should also fall at location 5, but instead the behavior corresponds to that found at location 4. Thus, in order to reconcile all the data it appears necessary to postulate two sets of curves, one for alloys with spherical particles, and one for alloys with platelets. Then the creep data at 6,000 psi for platelets would be shifted to location 3 in figure 20 without incurring any change in behavior, since locations 2 and 3 both fall in the intermediate-stress region. Therefore, the behavior of alloys with either spheres or platelets should be the same at 6,000 psi.

On the basis of the picture presented in figure 20, distinct differences due to particle shape should be expected in certain stress ranges. Because of the overlapping of some regions, the same behavior can be obtained in alloys with spherical particles as with platelets. Confirmation of the curves in reference 12, showing the relative strengths of alloys with fine and coarse spacings, was accomplished. Further verification of the scheme presented in figure 20 must await more extensive experimental investigation.

For both kinds of particles similar curves of matrix strength and measured strength at equal particle spacings were noted in spite of the particle-strengthening effects. This observation attests to the importance of solid-solution strengthening to alloy strength. Furthermore, it is shown that heavy precipitation can weaken an alloy because of the accompanying severe depletion of the matrix. By dissolution of the precipitate particles and consequent enrichment of the matrix, the strength of the particulate alloy approaches the calculated strength of a single-phase alloy with the same overall composition. Thus, the maximum

strengthening effect should be obtained when the matrix composition lies very near the saturation limit and when just enough precipitate has been formed for optimum strengthening of the alloy.

Comparisons With Theory

The results of the comparisons reported in this section are mostly negative in character, in that the available data did not conclusively validate or invalidate any theory of particle hardening. This was true primarily because a wide range of spacings was covered and different types of particles were investigated; the detailed scrutiny necessary to document any theoretically derived relationship was not performed.

However, the shape of the curves of particle strengthening versus spacing for spherical particles conforms to that generally expected; that is, the particle strengthening is greater at fine spacings and decreases up to the critical spacing. Thus, qualitative agreement with the ideas of Gensamer, Orowan, and Unckel were obtained, as well as with Dorn's data for aluminum-copper alloys.

A reexamination of the data of Hyam and Nutting revealed that Unckel's formulation was valid down to a spacing of about 0.5 micron. At smaller spacings a logarithmic plot of strength versus spacing was obeyed. A family of curves depending on alloy composition, as reported by Hyam and Nutting and by Shimura and Esser, was not noted in this investigation. Furthermore, separate curves would not be expected with the technique used here because subtracting the matrix strength from the measured strengths should give one curve independent of the overall alloy compositions.

The relationship advanced by Fisher, Hart, and Pry between particle radius and strengthening increment was not confirmed because of too much scatter in the critical plot. The restrictions imposed by their assumptions make it highly doubtful, however, that a satisfactory test of their theory will be obtainable with usual alloys.

On the other hand, it is possible that newer theories will be able to explain the increase in particle strengthening that occurs above the critical spacing. The enhanced strengths of alloys with coarser grain size, under certain conditions, must be closely related to the parallel effects observed with coarser particle spacings. A comprehensive theory should incorporate such features if it is to be effectively applied to high-temperature behavior.

Since no theories of particle hardening deal specifically with the effects of platelets on alloy strength, no comparisons with experiment can be reported. However, if the explanation advanced in the preceding

section to explain the different behavior of alloys with platelets is justified, a basis for a theoretical treatment may be at hand. Such a treatment should be based on considerations of strain energy due to the particle shape, with or without coherency strains. The theory should be able to account for the strains introduced by a superimposed stress, which may augment or diminish any internal strains. Explanations involving such factors as valency, temperature, or chemical effects, including the kinetics of precipitation and diffusion under an external stress, may conceivably utilize the methods of irreversible thermodynamics.

Under the complex situation existing in a particulate alloy, under stress, and at a high temperature, present-day theory cannot be expected to lead the way. Rather, by suitable experimental investigations, the important behavior patterns can be uncovered, thereby indicating the most fruitful directions for theoretical study.

CONCLUSIONS

The effects of controlled particle sizes and shapes on creep and tensile strengths have been investigated in aluminum-copper alloys over a wide range of particle spacings. Heat treatments were divised to yield particles closely approaching spheres; in other alloys, platelike particles were developed large enough to be resolved by the light microscope. Alloys with a wide range of matrix compositions were produced by overaging at different temperatures or by partially redissolving the precipitate in the single-phase region. Thus, unusually extreme combinations of matrix concentration and particle spacings are available for evaluation. The following results and conclusions were obtained from this investigation.

1. Quantitative metallographic techniques were applied to an evaluation of such particle characteristics as volume percent precipitation, mean spacings, mean radius, particle densities (per area or length). Certain of these characteristics are related, linearly when the precipitates are present in small amounts, which accounts for the adequacy of particle spacing for most correlations with strength properties.

2. Some evidence is marshalled in support of the unusual X-ray results obtained with alloys aged to produce platelike particles. Unexpectedly low copper contents in the matrix may be related to the anomalously high amounts of precipitate reported in this system, as well as to an unusual early expansion detected by dilation measurements. The transient character of these early precipitates may be connected with the loss in creep resistance that occurs in these alloys.

3. The hardening increment ascribable to particles is considered to be the difference between the strength of the particulate alloy and that of a single-phase alloy with the same composition as the matrix in the alloy. The effective copper content of the matrix is given by X-ray measurements. A calculated matrix strength, determined for the same conditions of temperature and stress as were used to test the specimen, is obtained from interpolated single-phase curves. Thus, the strengthening increment due to particles is evaluated. It appears that this technique may be useful with complex alloys, since it offers a way of clearly distinguishing between particle strengthening and strengthening due to solid-solution alloying.

4. A decrease in particle strengthening due to spherical particles occurs up to a critical spacing of about 50 microns; then, at larger spacings there is an increase to a large value at spacings near 500 microns. Previous investigators of particle strengthening effects did not study spacings greater than about 50 microns, so the increase in strength at wider spacings was not detected.

5. Although profuse stress-induced precipitation occurred during the creep tests, the strengthening curves derived from both creep and room-temperature tensile data followed qualitatively the same course when plotted against particle spacing. This similarity of shape implies that the effect of the initial microstructure persists throughout the test and is essentially unaffected by precipitation during creep.

6. Reversals in the relative strength of alloys with fine and coarse particle spacings were found to depend on the stress range in which the alloys were tested. For alloys with spacings less than the critical, at low and high stresses the alloys with finer spacings are stronger, and the opposite is true at intermediate stresses. Alloys with platelike particles appear to conform to the same type of scheme as do alloys with spherical particles; however, the stresses where the reversals take place appear to be slightly different.

7. For both kinds of particles similar curves of matrix strength and measured strength at equal particle spacings were noted in spite of the particle-strengthening effects. This observation attests to the importance of solid-solution strengthening to alloy strength. Furthermore, it is shown that heavy precipitation can weaken an alloy because of the accompanying severe depletion of the matrix. By dissolution of the precipitate particles and consequent enrichment of the matrix, the strength of the particulate alloy approaches the calculated strength of a single-phase alloy with the same overall composition. Thus, the maximum strengthening effect should be obtained when the matrix composition lies

very near to the saturation limit and when just enough precipitate has been formed for optimum strengthening of the alloy.

Battelle Memorial Institute,
Columbus, Ohio, May 31, 1957.

REFERENCES

1. Dorn, J. E., and Starr, C. D.: Effect of Dispersions on Mechanical Properties. ASM Seminar on Relation of Properties to Microstructure, 1954, pp. 71-94.

2. Gensamer, M., Pearsall, E. V., Pellini, W. S., and Low, J. R.: The Tensile Properties of Pearlite, Bainite, and Shperoidite. Trans. ASM, vol. 30, 1942, pp. 983-1020.

3. Roberts, C. S., Carruthers, R. C., and Averbach, B. L.: The Initiation of Plastic Strain in Plain and Carbon Steels. Trans. ASM, vol. 45, 1952, pp. 1150-1157.

4. Shaw, R. B., Shepard, L. A., Starr, C. D., and Dorn, J. E.: The Effect of Dispersions on Tensile Properties of Aluminum-Copper Alloys. Trans. ASM, vol. 45, 1953, pp. 249-271. Discussion by J. H. Westbrook, p. 273.

5. Shimura, S., and Esser, H.: Die Abhangigkeit der Harte bei Kohlenstoffstahlen von der Teilchengrosse des Eisenkarbides. Stahl und Eisen, Bd. 50, Heft 48, Nov. 27, 1930, pp. 1674-1675.

6. Hyam, E. D., and Nutting, J.: Tempering of Plain Carbon Steels. Jour. Iron and Steel Inst., vol. 184, pt. 2, Oct. 1956, pp. 148-165.

7. Keeler, J. H.: Tensile Properties of Zr-Cr Alloys - Particle-Strengthening Effects. Trans. ASM, vol. 48, no. 48, 1956, pp. 825-842.

8. Orowan, E.: Classification and Nomenclature of Internal Stresses. Symposium of Internal Stresses in Metals and Alloys, Inst. of Metals (London), 1948, discussion, p. 451-453.

9. Fisher, J. C., Hart, E. W., and Pry, R. H.: The Hardening of Metal Crystals by Precipitate Particles. Acta. Met., vol. 1, no. 3, May 1953, pp. 336-339.

10. Hibbard, W. R., Jr., and Hart, E. W.: Dispersion Hardening of Copper-Chromium Alloys. Jour. Metals, vol. 7, no. 1, sec. 2 (Trans.), Jan. 1955, pp. 200-202.

11. Reiter, S. F., and Hibbard, W. R., Jr.: High-Temperature Properties of Iron-Rich Fe-Mo Alloys. Jour. Metals, vol. 7, no. 5, sec. 2 (Trans.), May 1955, pp. 655-663.

12. Giedt, W. H., Sherby, O. D., and Dorn, J. E.: The Effect of Dispersions on Creep Properties of Aluminum-Copper Alloys. Trans. ASME, vol. 77, no. 1, Jan. 1955, pp. 57-62; discussion, pp. 62-63.

13. Underwood, E. E., Marsh, L. L., and Manning, G. K.: Creep of Aluminum-Copper Alloys During Age Hardening. NACA TN 4036, 1958.

14. Mott, N. F., and Nabarro, F. R. N.: Dislocation Theory and Transient Creep. Conf. on Strength of Solids, Phys. Soc. (London), 1948.

15. Unckel, H.: The Dependence of Mechanical Properties on Structure in Two-Phase Alloys. Metall., Bd. 5, Heft 7/8, Apr. 1951, pp. 146-150.

16. Howard, Robert T., and Cohen, Morris: Quantitative Metallography by Point-Counting and Lineal Analysis. Trans. AIME, vol. 172, 1947, pp. 413-426.

17. Scheil, E.: Die Berechnung der Anzahl und Grossenverteilung kugelformiger Kristalle in undurchsichtigen Korpen mit Hilfe der durch einen ebenen Schnitt erhaltenen Schnittkreise. Zs. anorg. und allgem. Chemie, Bd. 201, Heft 3/4, Dec. 8, 1931, pp. 259-264.

18. Schwartz, H. A.: Metallographic Determination of the Size Distribution of Temper Carbon Nodules. Metals and Alloys, vol. 5, no. 6, June 1934, pp. 139-140.

19. Lord, G. W., and Willis, T. F.: Calculation of Air Bubble Size Distribution from Results of a Roseival Traverse of Aerated Concrete. ASTM Bulletin, no. 177, Oct. 1951, pp. 56-61.

20. Fullman, R. L.: Measurement of Particle Sizes in Opaque Bodies. Trans. AIME, vol. 197, no. 3 , 1953, pp. 447-452.

21. Carreker, Roland P., Jr., and Hibbard, Walter R., Jr.: Tensile Deformation of Aluminum and a Function of Temperature, Strain Rate, and Grain Size. WADC Tech. Rep. 55-113, July 1955. Contract AF-33(616)-2120.

22. Carreker, Roland P., Jr., Guard, Ray W., and Lenhart, R. E.: Investigations of Deformation and Fracture of Metals. WADC Tech. Rep. 55-303, May 1955. Contract AF-33(616)-2120.

23. Manjoine, M. J.: High Temperature Properties of Materials. Proc. for a Short Course Conducted at Penn. State Univ., June 21-25, 1954.

24. Heimerl, George J.: Time-Temperature Parameters and Application to Rupture and Creep of Aluminum Alloys. NACA TN 3195, 1954.

25. Simmons, W. F., and Cross, H. C.: The Elevated-Temperature Properties of Selected Super-Strength Alloys. ASTM-ASME Joint Committee on Effect of Temperature on the Properties of Metals. ASTM Spec. Tech. Pub. 160, 1954.

26. Larson, F. R., and Miller, James: A Time-Temperature Relationship for Rupture and Creep Stresses. Trans. ASME, vol. 74, no. 5, July 1952, pp. 765-771.

27. Sherby, O. D., and Dorn, J. E.: Creep Correlations in Alpha Solid Solutions of Aluminum. Jour. Metals, vol. 4, no. 9, Sept. 1952, pp. 959-964.

28. Sherby, O. D., Anderson, R. A., and Dorn, J. E.: The Effect of Alloying Elements on the Elevated Temperature Plastic Properties of Alpha Solid Solutions of Aluminum. Trans. AIME, vol. 189, 1951, pp. 643-652.

29. Servi, I. S., and Grant, N. J.: Creep and Stress-Rupture Behavior of Aluminum as Function of Purity. Trans. AIME, vol. 191, 1951, pp. 909-916.

30. Gemmell, G. D., and Grant, N. J.: Effects of Solid Solution Alloying on Creep Deformation of Aluminum. Trans. AIME, vol. 209, 1957, pp. 417-423.

31. Willis, R. F.: Discussion on "The Air Requirements of Frost Resistant Concrete" by T. C. Powers. Proc. Highway Research Board, vol. 29, 1949, pp. 203-211.

32. Axon, H. J., and Hume-Rothery, W.: The Lattice Spacings of Solid Solutions of Different Elements in Aluminum. Proc. Roy. Soc. (London), ser. A, vol. 193, no. 1032, Apr. 22, 1958, pp. 1-24.

33. Freeman, James W., Frey, D. N., Reynolds, E. E., and White, A. E.: Super Creep Resistant Alloys. Symposium on Plasticity and Creep of Metals. Spec. Tech. Pub. No. 107, ASTM, 1954.

34. Allen, N. P.: Discussion on "Microstructure and Creep" by James W. Freeman and C. L. Corey. Symposium on Creep and Fracture of Metals at High Temperatures, (May 31-June 2, 1954) Nat. Phys. Lab. (London), 1956, pp.

35. Wilsdorf, Heinz, and Kuhlmann-Wilsdorf, Doris: An Experimental Study of Dislocations in Aluminum-Copper Alloys by Means of Precipitation. Conf. on Defects in Crystalline Solids. Internat. Union of Physics, and Inst. of Physics and Physical Society. Univ. of Bristol (London), July 1954.

36. Guarnieri, G. J., Miller, J., and Vawter, F. J.: The Effect of Sigma Phase on the Short-Time High-Temperature Properties of 25 Chromium - 20 Nickel Stainless Steel. Trans. ASM. vol. 42, 1950, pp. 981-1000.

37. Lankes, J. C., and Wassermann, G.: Die Volumenanderungen einer Aluminium-Kupfer-Leigierung Wahrend der einzelnen Standien der Entmischung. Zs. f. Metall., Bd. 41, Heft 11, Nov. 1950, pp. 381-391.

TABLE I.- SPECTROGRAPHIC AND CHEMICAL ANALYSIS OF

ALUMINUM-COPPER ALLOYS

Nominal composition, weight percent copper	Chemical analysis, weight percent copper	Spectrographic analysis, parts per million			
		Silicon (a)	Iron	Lead	Magnesium
1	0.99 1.04 1.05 1.04	20	20	(b)	1.0
2	2.04 2.07 2.07 2.04	20	(b)	(b)	1.0
3	3.05 3.08 2.95 3.14	20	(b)	(b)	1.0
4	4.03 4.07 4.14 4.11	20	(b)	20	1.0

[a]Silicon pickup possible from electrode.

[b]Not detected; less than 20 parts per million.

TABLE II.- CREEP DATA FOR ALUMINUM ALLOYS

Specimen	Heat treatment	Test temperature, °C	Initial creep stress, psi	Gage length, in.	Time of run, min	Elongation, percent	Minimum creep rate, percent/min (a)	ASTM grain size (b)		Vickers hardness	Remarks
								Gage section	Shoulders		
Alloys containing 1 percent copper											
1-2P1	Overaged 3 days at 300° C	300	2,400	2	37	~22	360 $\times 10^{-3}$	1	1	---	Stopped
1-2-4	Overaged 3 days at 300° C plus 15 min at 370° C	300	1,600	2	462	~16	26.8	0, 1	1	---	Stopped
1-2-3	----------do----------	300	2,000	2	1,150	~14	6.88	1, 2	1, 2	---	Stopped
1-2P2	----------do----------	300	2,400	2	26	~21	432	0, 1	1, 2	---	Stopped
1-4-1	10 min at 540° C plus 0 min at 300° C	200	2,400	1	14,526	~2	.008	-1, 0	---	---	Stopped
1-4-4	----------do----------	200	4,000	1	8,360	12.7	.466	-2, -1	---	---	Ruptured
1-4-8	10 min at 540° C plus 5 min at 300° C	200	4,000	1	252	12.6	232.0	-2, -1	---	---	Stopped
1-4-10	----------do----------	200	4,000	1	10,376	18.5	(.278)	-2, -1	---	---	Ruptured
1-4-13	10 min at 540° C plus 10 min at 300° C	200	4,000	1	3,349	20.2	1.38	-2, -1	---	---	Ruptured
1-4-18	10 min at 540° C plus 30 min at 300° C	200	4,000	1	2,075	25.5	5.6	-1, 0	---	---	Stopped
1-4-3	10 min at 540° C plus 0 min at 300° C	200	4,500	1	404	28.4	31.5	-1	---	---	Stopped
1-4-9	10 min at 540° C plus 5 min at 300° C	200	4,500	1	321	29.0	78.3	-1	---	---	Ruptured
1-4-19	10 min at 540° C plus 30 min at 300° C	200	4,500	1	497	44.7	67.5	-2, -1	---	---	Stopped
1-4-2	10 min at 540° C plus 0 min at 300° C	200	5,000	1	116	~35	202.5	-2, -1	---	---	Ruptured
1-4-6	10 min at 540° C plus 5 min at 300° C	200	5,000	1	87	23.8	148.5	-1, 0	---	---	Ruptured
1-4-11	10 min at 540° C plus 10 min at 300° C	200	5,000	1	112	39.1	208.8	-2, -1	---	---	Ruptured
1-4-16	10 min at 540° C plus 30 min at 300° C	200	5,000	1	152	29.1	138.5	-1, 0	---	---	Stopped
Alloys containing 2 percent copper											
2-3P1	Overaged 3 days at 351° C	300	2,400	2	105	~25	123 $\times 10^{-3}$	1, 2	---	---	Stopped
2-3P2	Overaged 3 days at 351° C plus 15 min at 415° C	300	2,400	2	265	~22	39.9	0, 1	---	---	Stopped
2-3P3	Overaged 3 days at 351° C plus 60 min at 415° C	300	2,400	2	1,303	~23	6.48	1, 2	---	---	Stopped
2-3P4	Overaged 3 days at 351° C plus 120 min at 415° C	300	2,400	2	---	~3	---	1, 2	---	---	Ruptured
2-4-1	20 min at 540° C plus 0 min at 351° C	200	7,500	1	7,343	5.8	.091	-1, -2	---	---	Ruptured
2-4-6	20 min at 540° C plus 5 min at 351° C	200	7,500	1	5,392	9.1	.188	-2, -1	---	---	Stopped
2-4-11	20 min at 540° C plus 10 min at 351° C	200	7,500	1	9,466	6.9	.085	-1, 0	---	---	Ruptured
2-4-16	20 min at 540° C plus 30 min at 351° C	200	7,500	1	11,867	7.2	.085	-1	---	---	Ruptured
2-4-4	20 min at 540° C plus 0 min at 351° C	200	8,000	1	4,268	8.9	.221	-3, -2	---	---	Ruptured
2-4-14	20 min at 540° C plus 10 min at 351° C	200	8,000	1	4,364	6.0	.169	-2, -1	---	---	Ruptured
2-4-19	20 min at 540° C plus 30 min at 351° C	200	8,000	1	4,825	6.7	.218	-2, -1	---	---	Ruptured
2-4-3	20 min at 540° C plus 0 min at 351° C	200	8,500	1	3,459	7.3	.410	0, -1	---	---	Ruptured
2-4-9	20 min at 540° C plus 5 min at 351° C	200	8,500	1	3,292	7.8	.407	-2, -1	---	---	Ruptured
2-4-13	20 min at 540° C plus 10 min at 351° C	200	8,500	1	1,913	7.7	.421	-2, -1	---	---	Ruptured
2-4-18	20 min at 540° C plus 30 min at 351° C	200	8,500	1	2,221	8.5	.416	-2, -1	---	---	Ruptured
[c]1-4-14	10 min at 540° C plus 10 min at 300° C	200	4,500	1	8,965	1.09	.0135	---	---	---	Stopped
Alloys containing 3 percent copper											
3-2P1	Overaged 3 days at 390° C	300	2,400	2	326	~23	27.5 $\times 10^{-3}$	1	---	---	Stopped
3-2P2	Overaged 3 days at 390° C plus 15 min at 470° C	300	2,400	2	3,655	8.5	.275	0, 1	---	---	Stopped
3-2P3	Overaged 3 days at 390° C plus 40 min at 470° C	300	2,400	2	18,961	1.7	.0522	1	---	---	Ruptured
3-2P4	Overaged 3 days at 390° C plus 60 min at 470° C	300	2,400	2	6,191	2.7	.122	0, 1	---	---	Stopped
3-1-2	30 min at 540° C plus 0 min at 390° C	200	9,000	1	3,399	1.2	.0875	-1	---	---	Ruptured
3-1-6	30 min at 540° C plus 5 min at 390° C	200	9,000	1	4,539	5.3	.242	-1, 0	---	---	Ruptured
3-1-11	30 min at 540° C plus 10 min at 390° C	200	9,000	1	4,977	4.3	.183	-1, -2	---	---	Ruptured
3-1-16	30 min at 540° C plus 30 min at 390° C	200	9,000	1	1,789	3.5	(.236-.393)	-1, -2	---	---	Ruptured
3-1-4	30 min at 540° C plus 0 min at 390° C	200	9,500	1	7,677	9.3	.1675	-1, -2	---	---	Ruptured
3-1-8	30 min at 540° C plus 5 min at 390° C	200	9,500	1	3,270	6.2	.486	-1, 0	---	---	Ruptured
3-1-13	30 min at 540° C plus 10 min at 390° C	200	9,500	1	2,927	5.1	.366	-1, -2	---	---	Ruptured
3-1-18	30 min at 540° C plus 30 min at 390° C	200	9,500	1	3,428	4.8	.378	-2	---	---	Ruptured
3-1-5	30 min at 540° C plus 0 min at 390° C	200	10,000	1	3,084	5.9	.387	-2	---	---	Ruptured
3-1-9	30 min at 540° C plus 5 min at 390° C	200	10,000	1	1,783	4.8	.694	-1	---	---	Ruptured
3-1-14	30 min at 540° C plus 10 min at 390° C	200	10,000	1	1,582	4.2	.566	0	---	---	Ruptured
3-1-19	30 min at 540° C plus 30 min at 390° C	200	10,000	1	550	6.4	5.57	0	---	---	Ruptured
3-1-3T	Overaged 3 days at 390° C plus 60 min at 540° C	480	200	1	2,715	19.8	(5.08-5.87)	---	---	---	Stopped
3-1-1T	----------do----------	480	602	1	85	37.6	214	---	---	---	Stopped

[a]Parentheses indicate doubtful values.
[b]Underlined values present to greatest extent.
[c]Alloy contained approximately 1.87 percent copper.

TABLE II.- CREEP DATA FOR ALUMINUM ALLOYS - Concluded

Specimen	Heat treatment	Test temperature, °C	Initial creep stress, psi	Gage length, in.	Time of run, min	Elongation, percent	Minimum creep rate, percent/min (a)	ASTM grain size (b)		Vickers hardness	Remarks
								Gage section	Shoulders		
	Alloys containing 4 percent copper										
4-2P1	Overaged 3 days at 420° C	300	2,400	2	670	~23	9.5×10^{-3}	0, 1	-----		Stopped
4-1-5T	Overaged 4.8 days at 420° C	300	2,800	1	642	~15	8.27	.67	-----		Stopped
4-1-1	----------do----------	300	3,200	1	422	~21	(17.3)	1	1		Stopped
4-1-2T	----------do----------	300	3,200	1	206	~11	32.2	1	1		Stopped
4-1-28T	Overaged 3 days at 420° C	300	3,200	1	20	~60	854	5.6	-----		Ruptured
4-2P2	Overaged 3 days at 420° C plus 15 min at 510° C	300	2,400	2	9,670	~3	.382	0, 1	-----	----	Ruptured
4-1-6T	15 min at 540° C plus overaged at 420° C plus 0 min at 510° C	300	2,400	1	4,450	~6	.243	1.5	1	43.6	Stopped
4-1-5T	----------do----------	300	2,800	1	2,100	~10	.450	1.5	1	42.9	Stopped
4-1-4T	----------do----------	300	3,200	1	1,775	~5	1.09	1	1	43.2	Ruptured
4-1-3S	----------do----------	300	3,200	1	438	~5	1.93	.65	-----	----	Stopped
4-1-37S	----------do----------	200	7,500	1	11,000	~1.8	.082	----	-----	----	Ruptured
4-1-4S	----------do----------	200	10,000	1	1,820	~2	.490	----	-----	----	Ruptured
4-1-14S	Overaged at 420° C plus 15 min at 540° plus 0 min at 510° C	300	2,400	1	2,586	~6	.328	0, 1	-----	----	Stopped
4-1-15S	----------do----------	300	2,800	1	1,373	9	.650	0, 1	-----	----	Stopped
4-1-16S	----------do----------	300	3,200	1	1,663	3	.550	0, 1	-----	----	Ruptured
4-1-9T	15 min at 540° C plus overaged at 420° C plus 12 min at 510° C	300	2,400	1	3,400	~2.0	.142	.33	0	40.9	Power off during test
4-1-8T	----------do----------	300	2,800	1	2,973	~3.0	.375	.67	1	42.1	Stopped
4-1-7T	----------do----------	300	3,200	1	1,915	~4.0	.615	.5	1	44.2	Stopped
4-1-29	Overaged at 420° C plus 15 min at 540° C plus 12 min at 510° C	300	2,400	1	8,932	~6.7	.090	0, 1	-----	----	Stopped
4-1-17S	----------do----------	300	2,400	1	3,507	3.5	.147	-1	-----	----	Ruptured (rerun)
4-1-28	----------do----------	300	2,800	1	1,467	~7.3	.62	0, 1	-----	----	Stopped
4-1-27	----------do----------	300	3,200	1	740	2.5	1.28	0, 1	-----	----	Ruptured
4-1-12T	15 min at 540° C plus overaged at 420° C plus 30 min at 510° C	300	2,400	1	4,752	~3.0	.141	-.5	0	40.2	Stopped
4-1-11T	----------do----------	300	2,800	1	4,200	3.0	.41	.33	1	38.7	Ruptured
4-1-10T	----------do----------	300	3,200	1	750	<1.8	.92	-.33	-----	45.5	Ruptured
4-1-25T	Overaged at 420° C plus 15 min at 540° C plus 30 min at 510° C	200	9,000	1	6,127	~1.97	.147	-1, 0	-----	----	Interrupted for metallographic observation
4-1-26T	----------do----------	200	9,000	1	2,863	1.05	.108	0, 1	-----	----	Do.
4-1-27T	----------do----------	200	9,000	1	1,413	.92	----------	-1, 0	-----	----	Do.
4-4-24S	----------do----------	300	2,400	1	1,645	~3.2	.311	0, 1	-----	----	Stopped
4-1-30T	----------do----------	300	2,400	1	220	.85	.1435	0, 1	-----	----	Interrupted for metallographic observation
4-1-30T	----------do----------	300	2,400	1	1,332	1.02	.1435	0, 1	-----	----	Do.
4-1-29T	----------do----------	300	2,400	1	2,565	1.28	.1433	.5	-----	----	Do.
4-1-23S	----------do----------	300	2,800	1	-700	~6.0	.76	0, 1	-----	----	Ruptured
4-1-25S	----------do----------	300	3,200	1	400	~2.0	1.85	0, 1	-----	----	Ruptured
4-1-15T	15 min at 540° C plus overaged at 420° C plus 90 min at 510° C	300	2,400	1	7,585	~3.5	.091	-1.3	-1	39.2	Stopped
4-1-14T	----------do----------	300	2,800	1	3,223	~4.1	.28	-1	0, -1	42.6	Ruptured
4-1-13T	----------do----------	300	3,200	1	3,613	~4.5	.363	-1	-1	43.0	Stopped
4-1-22S	Overaged at 420° C plus 15 min at 540° C plus 90 min at 510° C	300	2,400	1	1,165	~9.6	.375	-1, 0	-----	----	Stopped
4-1-39T	----------do----------	300	2,400	1	9,847	1.65	.0424	0, 1	-----	----	Stopped
4-1-20S	----------do----------	300	2,800	1	1,200	~2	.117-.43	0, 1	-----	----	Ruptured
4-1-18S	Overaged at 420° C plus 15 min at 540° C plus 95 min at 510° C	300	2,800	1	4,450	~3	.169	-1, 0	-----	----	Ruptured
4-1-21S	Overaged at 420° C plus 15 min at 540° C plus 90 min at 510° C	300	3,200	1	300	~6	1.85	0	-----	----	Stopped
4-1-19S	----------do----------	300	3,200	1	1,750	11	.750	-2 -1	-----	----	Stopped
4-1-40S	----------do----------	200	7,500	1	15,700	1.4	.038	-----	-----	----	Stopped
4-1-38S	----------do----------	200	10,000	1	3,290	2	.250	0, 1	-----	----	Ruptured
4-1-8S	30 min at 540° C plus 12 min at 420° C	200	3,200	1	16,866	.5	.00347	0	-----	----	Stopped
4-1-12S	----------do----------	200	7,500	1	-9,000	2.7	.068	0	-----	----	Ruptured
4-1-11S	----------do----------	200	10,000	1	1,300	~3.5	1.0-1.56	0, 1	-----	----	Ruptured
4-1-9S	----------do----------	250	3,200	1	9,604	1.1	.0313	0, 1	-----	----	Stopped
4-1-10S	----------do----------	250	5,000	1	-3,400	~4.2	.205	0	-----	----	Ruptured
4-1-13S	----------do----------	250	7,500	1	-300	~6	6.27	0	-----	----	Ruptured
4-1-7S	----------do----------	300	2,400	1	605	~3	1.35	0, 1	-----	----	Stopped
4-1-5S	----------do----------	300	2,800	1	471	~2	1.80	0	-----	----	Stopped
4-1-6S	----------do----------	300	3,200	1	165	~11	7.8-8.7	-----	-----	----	Stopped
4-1-16T	Overaged at 420° C plus 60 min at 540° C	500	200	1	483	8.6	9.16	-3, -2	-----	----	Stopped
4-1-23T	----------do----------	500	600	1	48	28.0	234.8	-----	-1	----	Stopped

[a]Parentheses indicate doubtful values.
[b]Underlined values present to greatest extent.

TABLE III.- TENSILE DATA

Specimen	Heat treatment	Test temperature, °C	Strain rate per min	Gage length, in.	Elongation, percent	Ultimate tensile stress, psi	Average Vickers hardness at 10 kg load	ASTM grain size (a)	Phase
1-4-21	Overaged 4.2 days at 300° C	28	0.0318	1	31	13,260	24.8	------	θ
1-4-22	Overaged 4.2 days at 300° C plus 15 min at 370° C	28	.0318	1	30	14,040	26.8	------	θ
1-4-23	10 min at 540° C plus 0 min at 300° C	28	.0318	1	39.5	16,000	28.9	0	θ'
1-4-24	10 min at 540° C plus 5 min at 300° C	28	.0318	1	37	12,480	26.0	-2, -1	θ'
1-4-25	10 min at 540° C plus 10 min at 300° C	28	.0318	1	36	12,870	26.0	-1, 0	θ'
1-4-26	10 min at 540° C plus 30 min at 300° C	28	.0318	1	34.5	12,590	25.2	-1	θ'
1-4-1r	Overaged 3 days at 300° C plus 30 min at 540° C	27	.0318	1.5	----	14,370	----	-2	Single
1-4-6r	Overaged 3 days at 300° C plus 30 min at 540° C	100	.0318	1.5	----	11,820	----	-2, -3	Single
1-4-7r	Overaged 3 days at 300° C plus 30 min at 540° C	380	.0318	1.5	----	1,340	----	-2, -3	Single
1-4-10r	Overaged 3 days at 300° C plus 30 min at 540° C	480	.0318	1.5	----	660	----	-2, -1	Single
1-4-9r	Overaged 3 days at 300° C plus 30 min at 540° C	415	.0318	1.5	----	1,000	----	-2	Single
2-4-21	Overaged 4.3 days at 351° C	28	.0318	1	----	17,240	32.1	------	θ
2-4-23	Overaged 4.3 days at 351° C plus 15 min at 415° C	28	.0318	1	----	26,070	43.5	------	θ
2-4-24	Overaged 4.3 days at 351° C plus 60 min at 415° C	28	.0318	1	----	26,910	48.2	------	θ
2-4-22	Overaged 4.3 days at 351° C plus 120 min at 415° C	28	.0318	1	----	29,070	52.8	------	θ
2-4-25	20 min at 540° C plus 0 min at 351° C	28	.0318	1	----	27,690	71.2	-1	θ'
2-4-26	20 min at 540° C plus 5 min at 351° C	28	.0318	1	----	26,490	54.5	-1	θ'
2-4-27	20 min at 540° C plus 10 min at 351° C	28	.0318	1	----	26,280	53.0	-1	θ'
2-4-28	20 min at 540° C plus 30 min at 351° C	28	.0318	1	----	24,170	51.7	-2	θ'
3-1-21	Overaged 4.6 days at 390° C	28	.0318	1	----	25,170	44.2	------	θ
3-1-22	Overaged 4.6 days at 390° C plus 15 min at 470° C	28	.0318	1	----	33,870	64.6	2	θ
3-1-23	Overaged 4.6 days at 390° C plus 40 min at 470° C	28	.0318	1	----	33,890	59.3	1	θ
3-1-24	Overaged 4.6 days at 390° C plus 60 min at 470° C	28	.0318	1	----	35,010	68.8	1	θ
3-1-25	30 min at 540° C plus 0 min at 390° C	28	.0318	1	----	34,090	89.0	-1	θ'
3-1-26	30 min at 540° C plus 5 min at 390° C	28	.0318	1	----	34,010	81.4	-1, 0	θ'
3-1-27	30 min at 540° C plus 10 min at 390° C	28	.0318	1	----	32,210	76.9	-2, -1	θ'
3-1-28	30 min at 540° C plus 30 min at 390° C	28	.0318	1	----	31,090	63.4	-2, -1	θ'
3-1-8r	Overaged 3 days at 390° C plus 60 min at 540° C	27	.0318	1.5	----	34,000	----	-1	Single
3-1-4r	Overaged 3 days at 390° C plus 60 min at 540° C	100	.0318	1.5	----	26,000	----	-3, -2	Single
3-1-6r	Overaged 3 days at 390° C plus 60 min at 540° C	480	.0318	1.5	----	1,090	----	-2, -1	Single
3-1-7r	Overaged 3 days at 390° C plus 60 min at 540° C	520	.0318	1.5	----	750	----	-1	Single
3-1-10r	Overaged 3 days at 390° C plus 60 min at 540° C	550	.0318	1.5	----	590	----	-2	Single
4-1-33	Overaged 4.6 days at 420° C	28	.0318	1	31.3	30,570	49.5	------	θ
4-1-31	Overaged 3 days at 420° C plus 15 min at 540° C plus 0 min at 510° C	28	.0108	1	30.4	39,470	62.5	0	θ_{II}
4-1-32	Overaged 3 days at 420° C plus 15 min at 540° C plus 12 min at 510° C	28	.0108	1	25.0	37,980	52.0	-1	θ_{II}
4-1-33	Overaged 3 days at 420° C plus 15 min at 540° C plus 30 min at 510° C	28	.0108	1	28.3	39,470	66.9	-1	θ_{II}
4-1-34	Overaged 3 days at 420° C plus 15 min at 540° C plus 90 min at 510° C	28	.0108	1	26.1	43,080	63.3	-1, -2	θ_{II}
4-1-30	30 min at 540° C plus 12 min at 420° C	28	.0108	1	32.8	37,100	58.0	------	θ'
4-1-17r	Overaged 3 days at 420° C plus 60 min at 540° C	27	.0318	1.5	----	41,280	----	-1, 0	Single
4-1-18r	Overaged 3 days at 420° C plus 60 min at 540° C	100	.0318	1.5	----	35,080	----	0	Single
4-1-21r	Overaged 3 days at 420° C plus 60 min at 540° C	500	.0318	1.5	----	980	----	-1	Single
4-1-22r	Overaged 3 days at 420° C plus 60 min at 540° C	520	.0318	1.5	----	800	----	-1	Single
4-1-24r	Overaged 3 days at 420° C plus 60 min at 540° C	550	.0318	1.5	----	640	----	-1	Single

[a]Underlined values present to greatest extent.

TABLE IV.- X-RAY RESULTS

Type of particle	Sample	Nominal Cu, wt. percent	Heat treatment	Matrix composition, wt. percent copper		Chemical analysis, wt. percent copper
				Filings	Bulk specimens	
	1	1	Annealed	0.82	----	[a]1.05
	2	2	Annealed	1.95	----	[a]2.06
	3	3	Annealed	3.42	----	[a]3.19
	4	4	Annealed	4.18	----	[a]4.15
Spherical particles						
θ	1-A	1	Overaged	1.28	1.20	----------
	1-B	1	Overaged plus 15 min	.95	1.19	[b]0.96 to 0.98
	2-A	2	Overaged	.91	.91	----------
	2-B	2	Overaged plus 15 min	1.28	1.33	[b]1.80 to 2.00
	3-A	3	Overaged	2.09	2.28	----------
	3-B	3	Overaged plus 15 min	3.52	3.32	[b]2.70 to 2.80
	4-A	4	Overaged	1.62	1.71	----------
	4-B	4	Overaged plus 15 min	2.61	2.71	[b]3.40 to 3.70
θ_I	10-A	4	0 min at 510° C	----	3.28	
	10-B	4	12 min at 510° C	----	3.32	
	10-C	4	30 min at 510° C	----	2.75	
	10-D	4	90 min at 510° C	----	3.23	
θ_{II}	8-A	4	0 min at 510° C	3.80	3.75	
	8-B	4	12 min at 510° C	4.51	3.38	
	8-C	4	30 min at 510° C	3.56	2.99	
	8-D	4	90 min at 510° C	4.04	2.85	
Platelike particles						
θ'	5-A	1	Aged 0 min at 300° C	----	0.76	
	5-B	1	Aged 5 min at 300° C	----	1.76	
	5-C	1	Aged 10 min at 300° C	----	----	
	5-D	1	Aged 30 min at 300° C	----	1.66	
	6-A	2	Aged 0 min at 350° C	2.70	----	
	6-B	2	Aged 5 min at 350° C	1.33	----	
	6-C	2	Aged 10 min at 350° C	1.19	----	
	6-D	2	Aged 30 min at 350° C	2.09	----	
	7-A	3	Aged 0 min at 390° C	2.56	----	
	7-B	3	Aged 5 min at 390° C	.44	----	
	7-C	3	Aged 10 min at 390° C	4.32	3.80	
	7-D	3	Aged 30 min at 390° C	----	----	
	9-A	4	Aged 12 min at 420° C	4.37	----	

[a]Analyzed by wet chemical methods.

[b]Analyzed spectrographically.

TABLE V.- PARTICLE CHARACTERISTICS

(a) Spherical particles

Type of particle	Nominal Cu, wt. percent	Solution time	Volume fraction, f (a)	Mean center-to-center spacing, S, mm	Mean free path, λ, mm (b)	Mean radius of spherical particles, $\bar{r}$, mm (c)	Analysis according to reference 17: Number of particles per cu mm	Analysis according to reference 17: $\bar{r}$ of sphere with mean volume	Analysis according to reference 17: Volume fraction, f	Volume fraction, f, analysis according to ref. 19
θ_I	4	0	0.953	0.380	0.378	2.72×10^{-3}	----------	----------	-----	-----
		12	.748	.457	.453	2.56	----------	----------	-----	-----
		30	.842	.479	.474	3.03	----------	----------	-----	-----
		60	.523	.559	.556	2.19	----------	----------	-----	-----
		120	.250	1.92	1.92	3.60	----------	----------	-----	-----
		6	1.351	.216	.216	2.19	----------	----------	-----	-----
		20	1.380	.315	.311	3.26	----------	----------	-----	-----
		42	.760	.490	.486	2.79	----------	----------	-----	-----
		52	.917	.579	.573	3.98	----------	----------	-----	-----
		90	.719	.546	.542	2.94	----------	----------	-----	-----
θ_{II}	4	0	.791	.558	.554	3.31	1.58×10^5	1.216×10^{-3}	0.813	0.816
		12	.604	.662	.658	3.00	2.05	.835	.687	.736
		30	.711	.629	.626	4.72	1.01	1.223	.508	.738
		90	.594	.539	.536	2.40	1.62	.920	.588	.624
θ	1	0	.658	.0432	-----	.213	----------	----------	-----	-----
	1	15	.469	.0406	-----	.143	----------	----------	-----	-----
	2	0	1.39	.0102	-----	.106	----------	----------	-----	-----
	2	15	.918	.0178	-----	.123	----------	----------	-----	-----
	3	0	2.02	.0122	-----	.185	----------	----------	-----	-----
	3	15	.509	.0459	-----	.175	----------	----------	-----	-----
	4	0	2.64	.0275	-----	.545	----------	----------	-----	-----
	4	15	1.43	.1887	-----	2.024	----------	----------	-----	-----

(b) Platelike θ' particles

Nominal Cu, wt. percent	Aging time, min	S, mm	Relative volume percent	Linear density per mm: Calc.	Linear density per mm: Measured at X1500	Calc. N_V per cu mm	Thickness, mm	Ratio of diameter to thickness
1	0	[d]0.00308	----	-----	-----	----------	----------	----
	5	[d].00145	----	-----	-----	----------	----------	----
	10	[d].00142	----	-----	-----	----------	----------	----
	30	[d].00146	----	-----	-----	----------	----------	----
2	0	.209	----	-----	-----	----------	----------	----
	5	.075	3.85	113.8	200.5	2205×10^5	0.169×10^{-3}	8.6
	10	.057	2.31	68.4	221.0	3700	.169	5.7
	30	.011	2.92	86.3	118.0	2555	.169	6.8
3	0	.046						
	5	.015	10.09	298.0	480.0	7410	.169	7.3
	10	.014	11.28	222.0	392.0	6180	.254	4.93
	30	.010	7.61	150.0	227.0	5180	.254	4.33
4	12	.0099	8.69	128.3	194.5	1880	.338	4.33

[a] Derived for θ_I and θ_{II} by linear analysis; calculated for θ.

[b] $\lambda = (1 - f)/N_L$.

[c] $\bar{r} = \frac{3}{4}fS$.

[d] S measured at X18,000.

TABLE VI.- HEAT TREATMENTS OF ALUMINUM-COPPER ALLOYS FOR OBTAINING VARIOUS PARTICLE CHARACTERISTICS

Particle type produced	Copper content, percent	Heat treatment
Heat treatments of θ particles at solvus temperatures		
Spherical	1	Overaged 3 days at 300° C plus 0 or 15 min at 370° C
	2	Overaged 3 days at 351° C plus 0, 15, 60, or 120 min at 415° C
	3	Overaged 3 days at 390° C plus 0, 15, 40, or 60 min at 470° C
	4	Overaged 3 days at 420° C plus 0 or 15 min at 510° C
Special heat treatments of θ particles in 4-percent-copper alloys		
Spherical, θ_I [a]	4	15 min at 540°, overaged 4.75 days at 420° C, plus 0, 12, 30, or 90 min at 510° C
Spherical, θ_{II} [b]		Overaged 3 days at 420° C, 15 min at 540° C, plus 0, 12, 30, or 90 min at 510° C
Heat treatments of θ' particles		
Platelike	1	10 min at 540° C plus 0, 5, 10, or 30 min at 300° C
	2	20 min at 540° C plus 0, 5, 10, or 30 min at 351° C
	3	30 min at 540° C plus 0, 5, 10, or 30 min at 390° C
	4	30 min at 540° C plus 12 min at 420° C

[a] θ_I particles were produced by aging before high-temperature treatment.

[b] θ_{II} particles were produced by aging after high-temperature treatment.

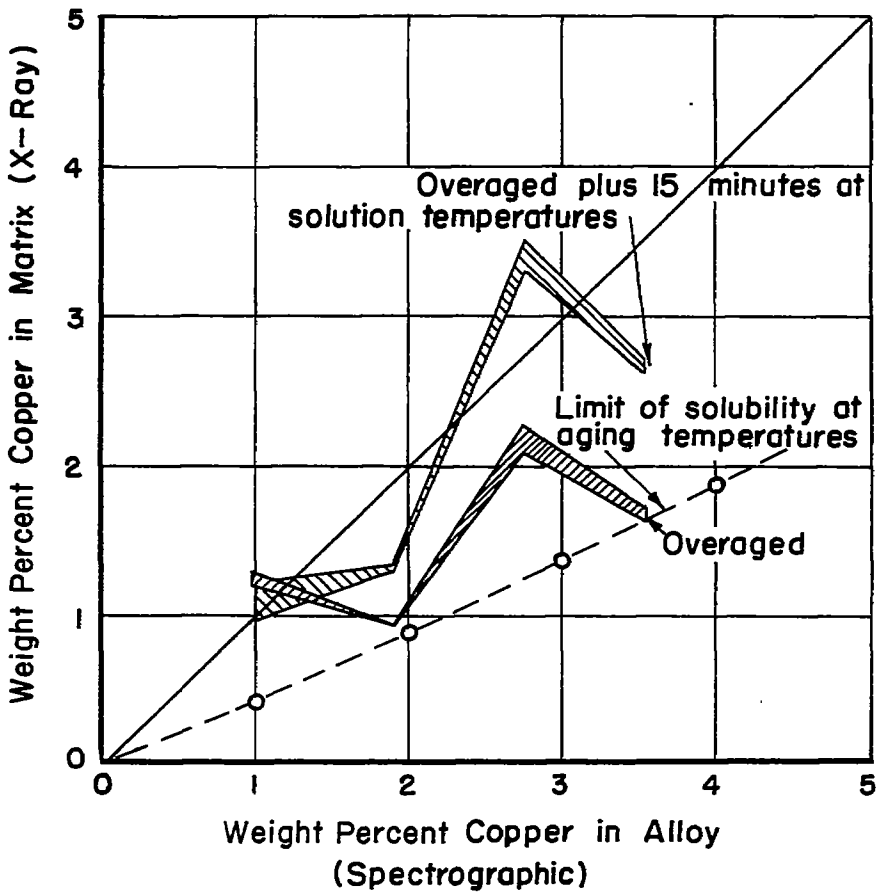

Figure 1.- X-ray measurements of matrix lattice parameters in overaged aluminum-copper alloys.

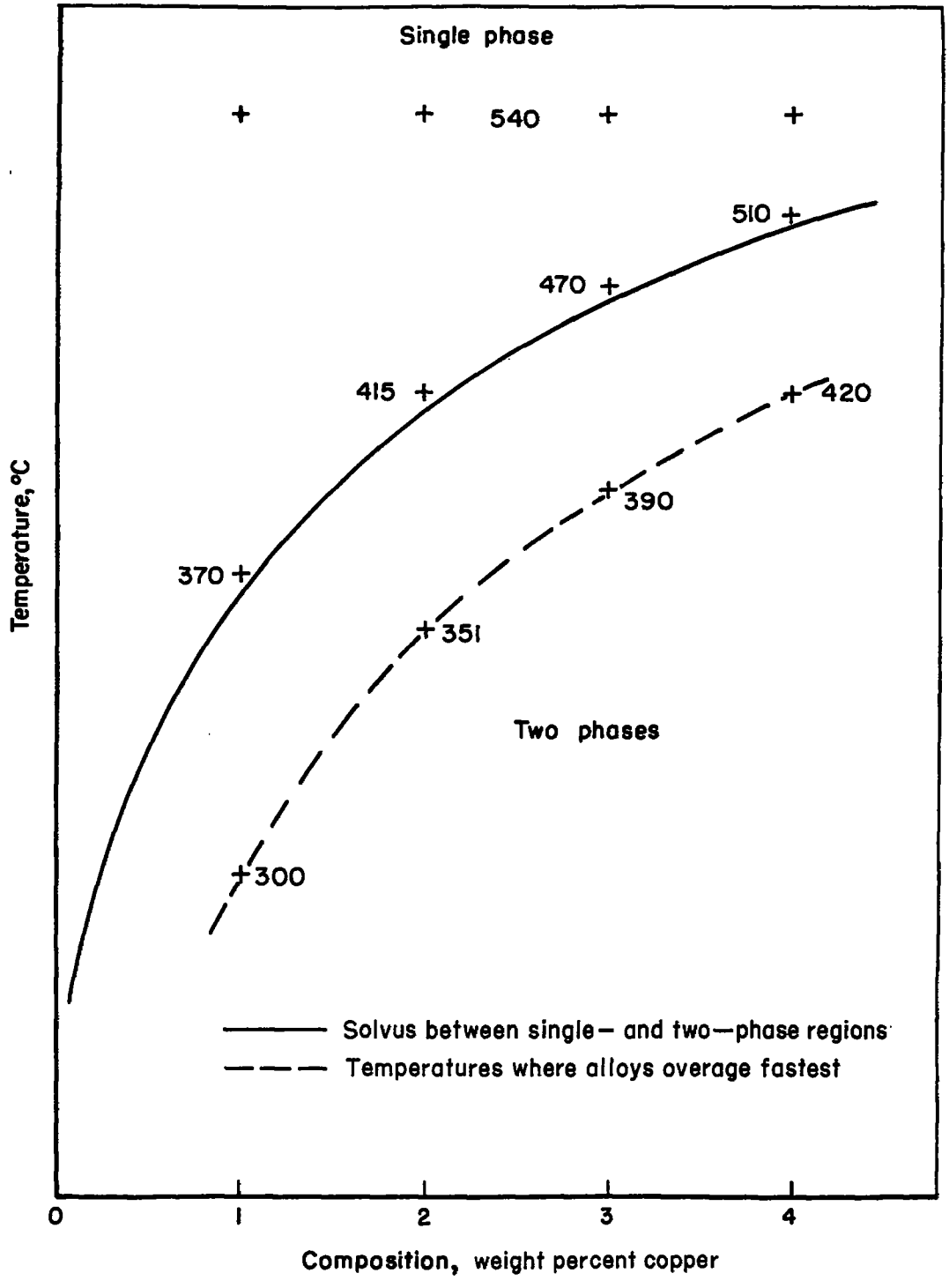

Figure 2.- Heat-treatment temperatures for aluminum-copper alloys.

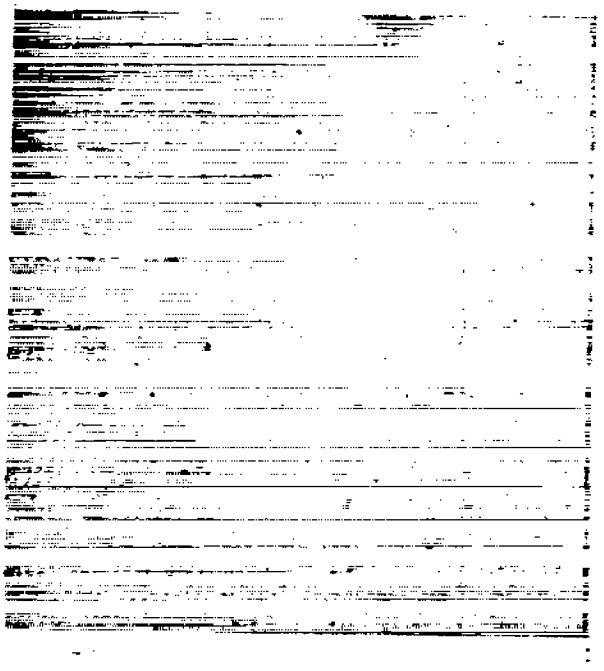

(a) θ_{II} structure, 0 minute at 510° C; unetched; X100.

(b) θ_{II} structure; etching solution, 1.5 cubic centimeters hydrochloric acid, 3.5 cubic centimeters nitric acid, and 195 cubic centimeters water; crept at 200° C under 7,500 psi; X50.

(c) θ_{I} structure; 90 minutes at 510° C; Keller's etch; X250.

Figure 3.- Spherical precipitate particles in aluminum alloys containing 4 percent copper.

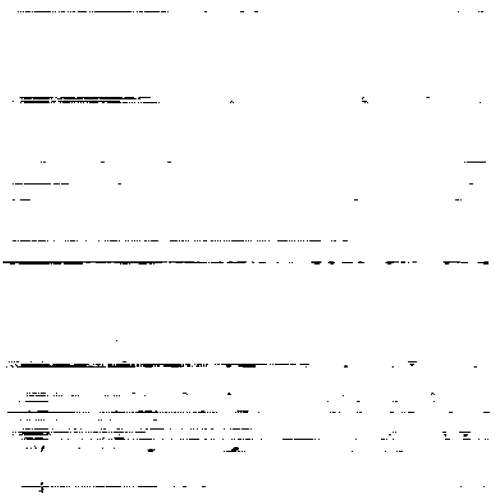

(a) 4 percent copper; 30 minutes at 350° C.

(b) 3 percent copper; 30 minutes at 390° C.

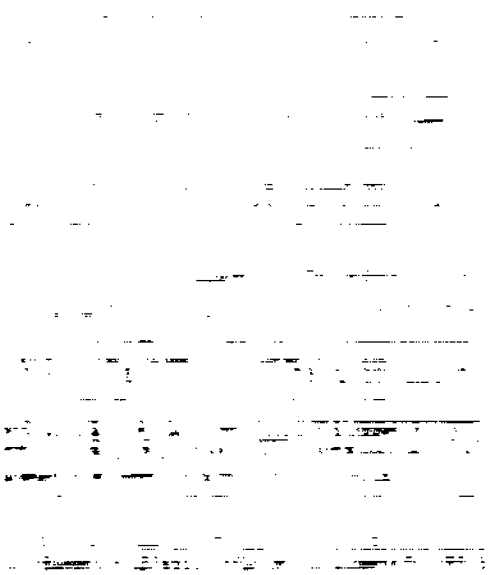

(c) 4 percent copper; 12 minutes at 420° C.

Figure 4.- Platelike particles of θ' structure in aluminum-copper alloys before creep testing; Keller's etch; X1,500.

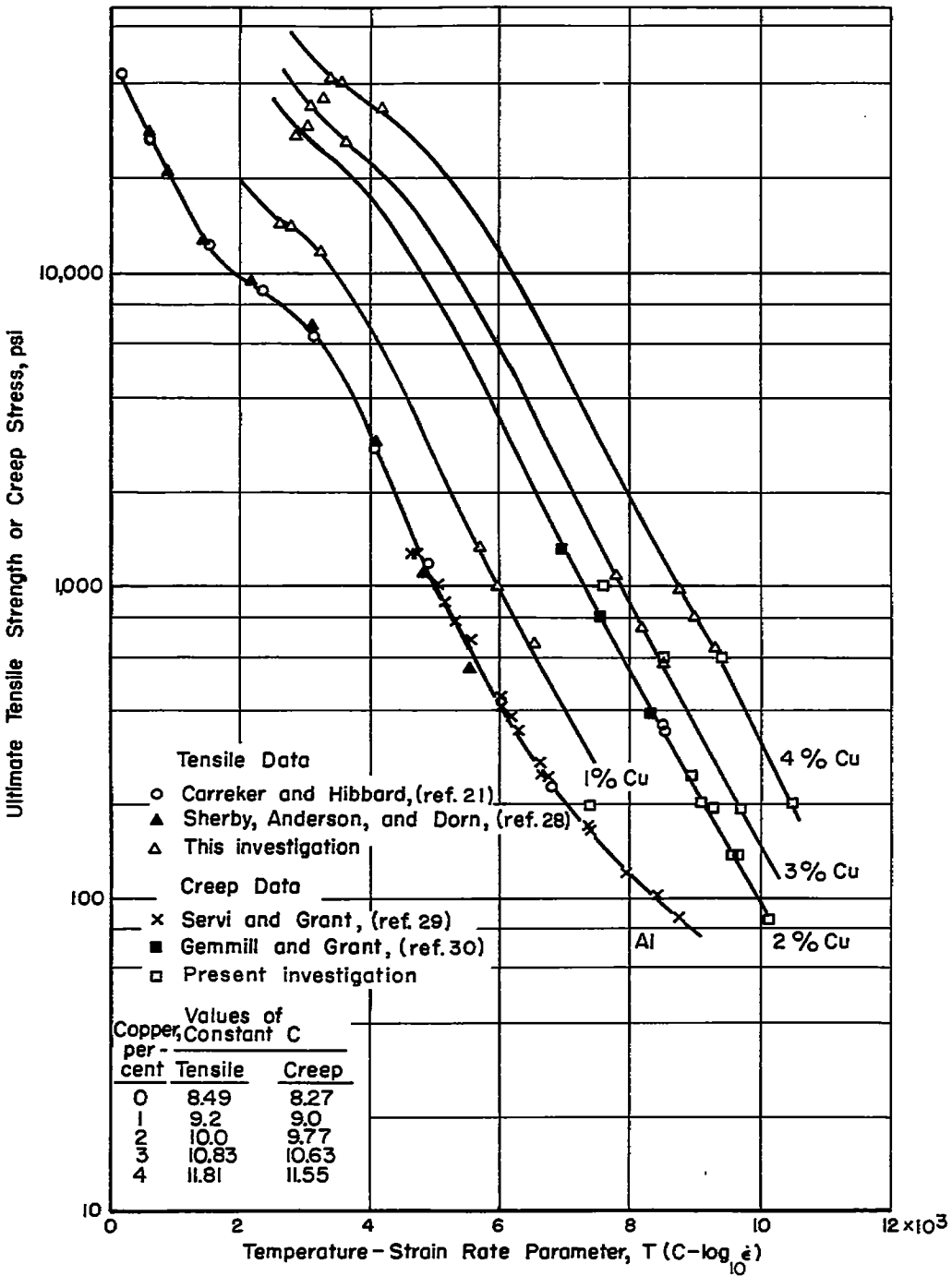

Figure 5.- Tensile and creep data for single-phase aluminum-copper alloys interpolated into two-phase region of equilibrium diagram. T is in °K; strain rate $\dot{\epsilon}$ is in percent per minute.

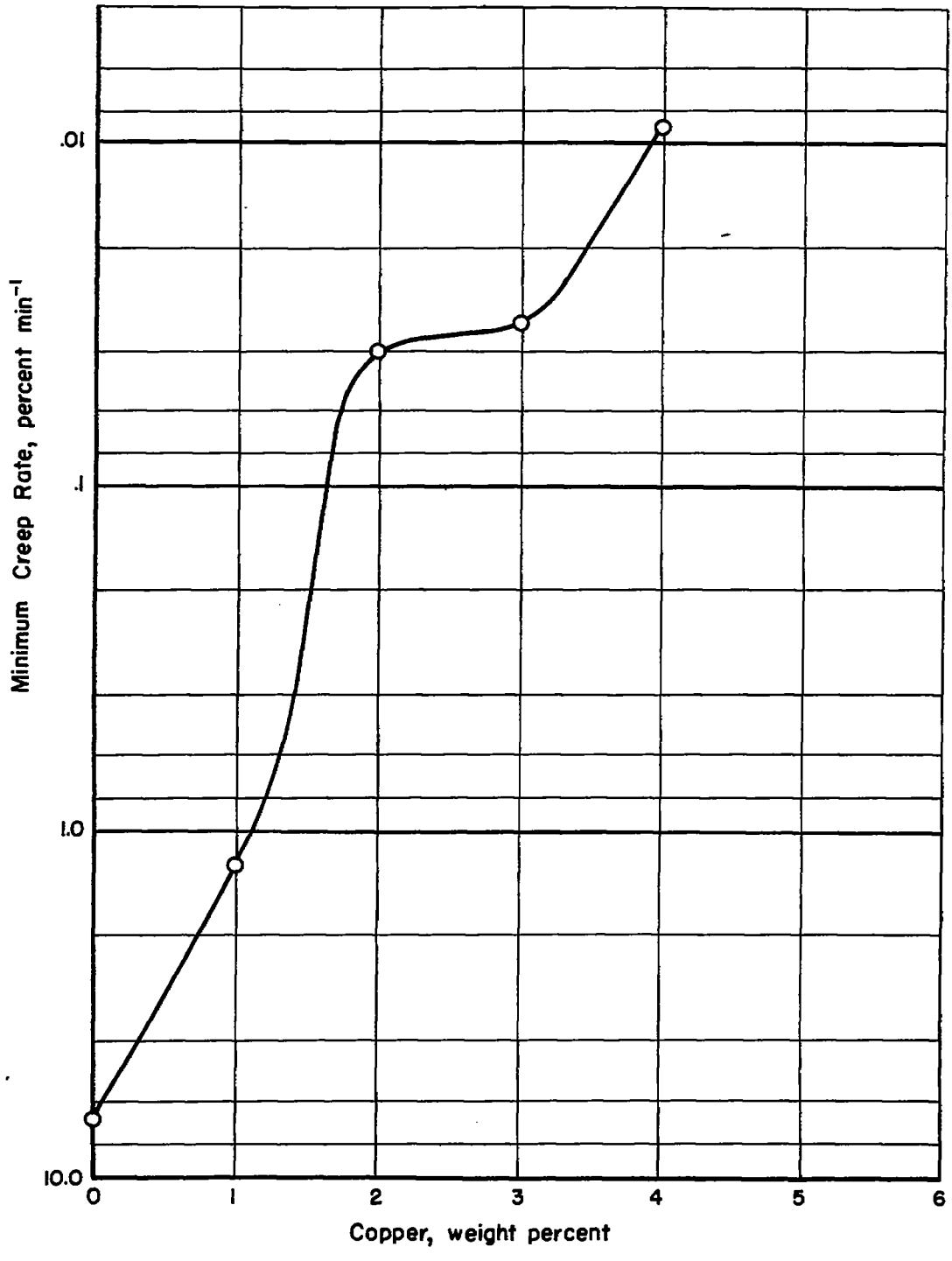

Figure 6.- Minimum creep rate versus composition for metastable single-phase aluminum-copper alloys at 300° C and 2,400 psi.

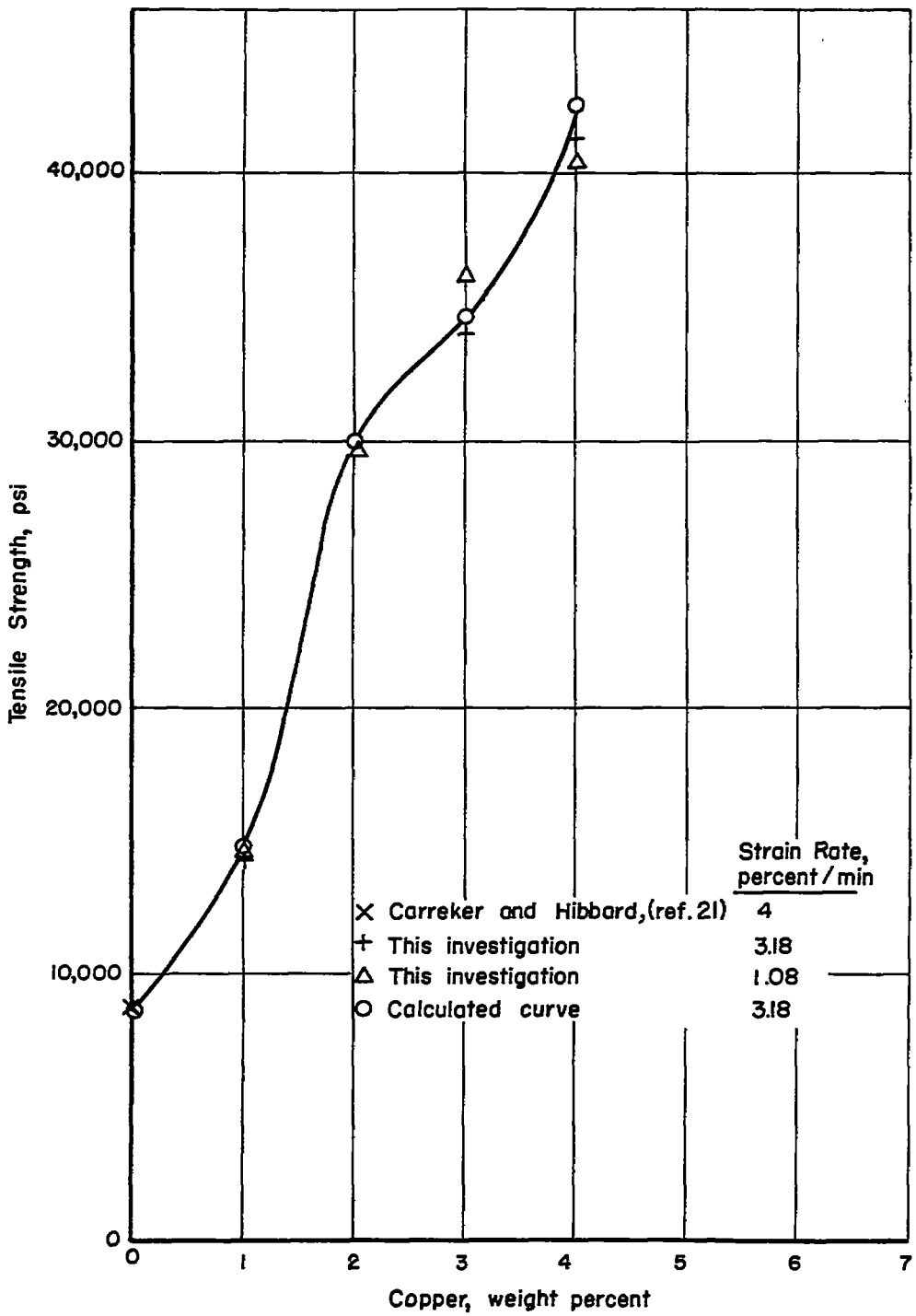

Figure 7.- Measured and calculated room-temperature tensile strengths of single-phase aluminum-copper alloys.

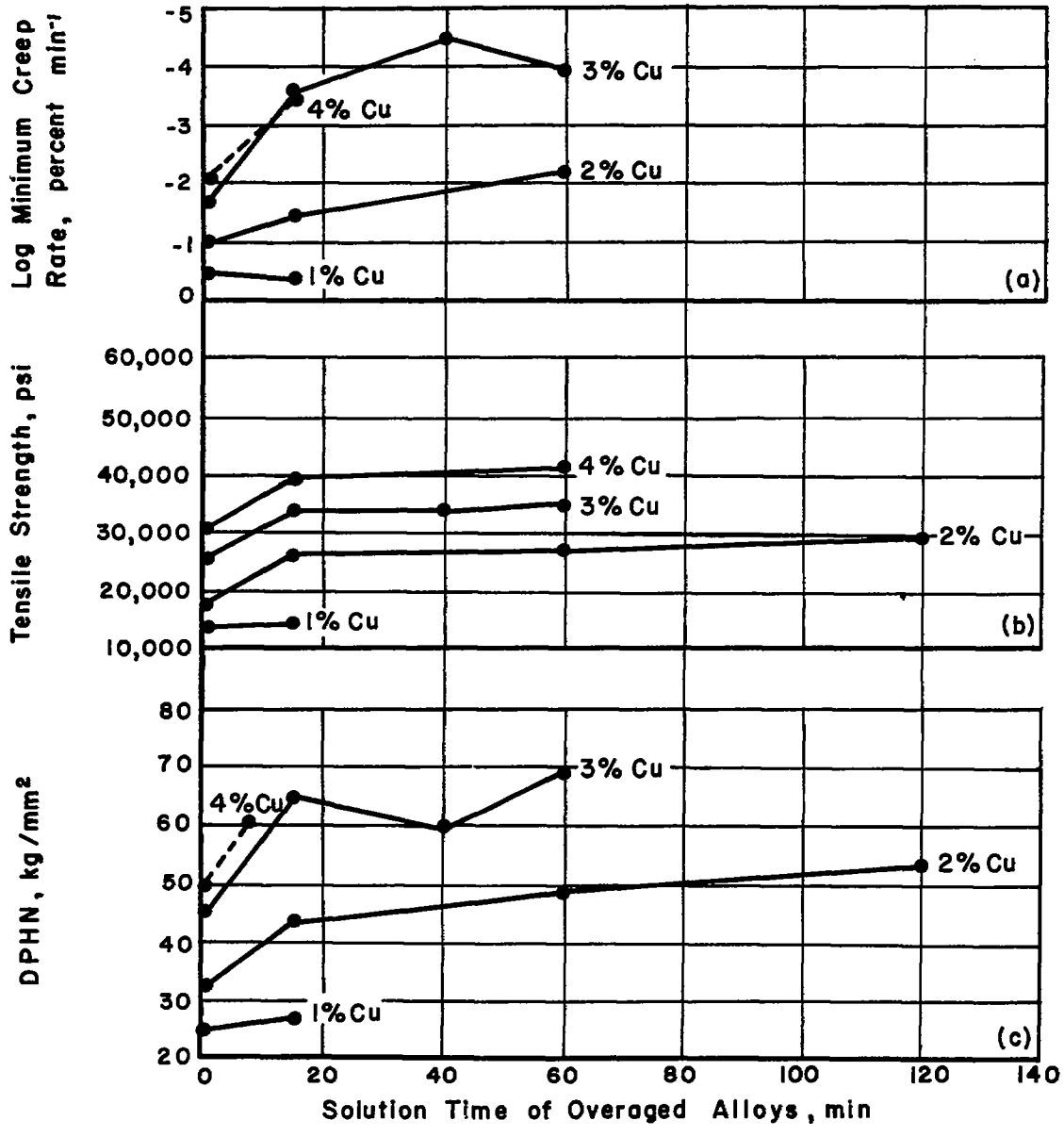

(a) Creep data tested at 300° C under 2,400 psi.

(b) Tensile strength measured at room temperature. $\dot{\epsilon}$ = 3.18 percent per minute.

(c) Hardness values measured at root temperature.

Figure 8.- Change in properties of overaged aluminum-copper alloys after solution treatments for various times.

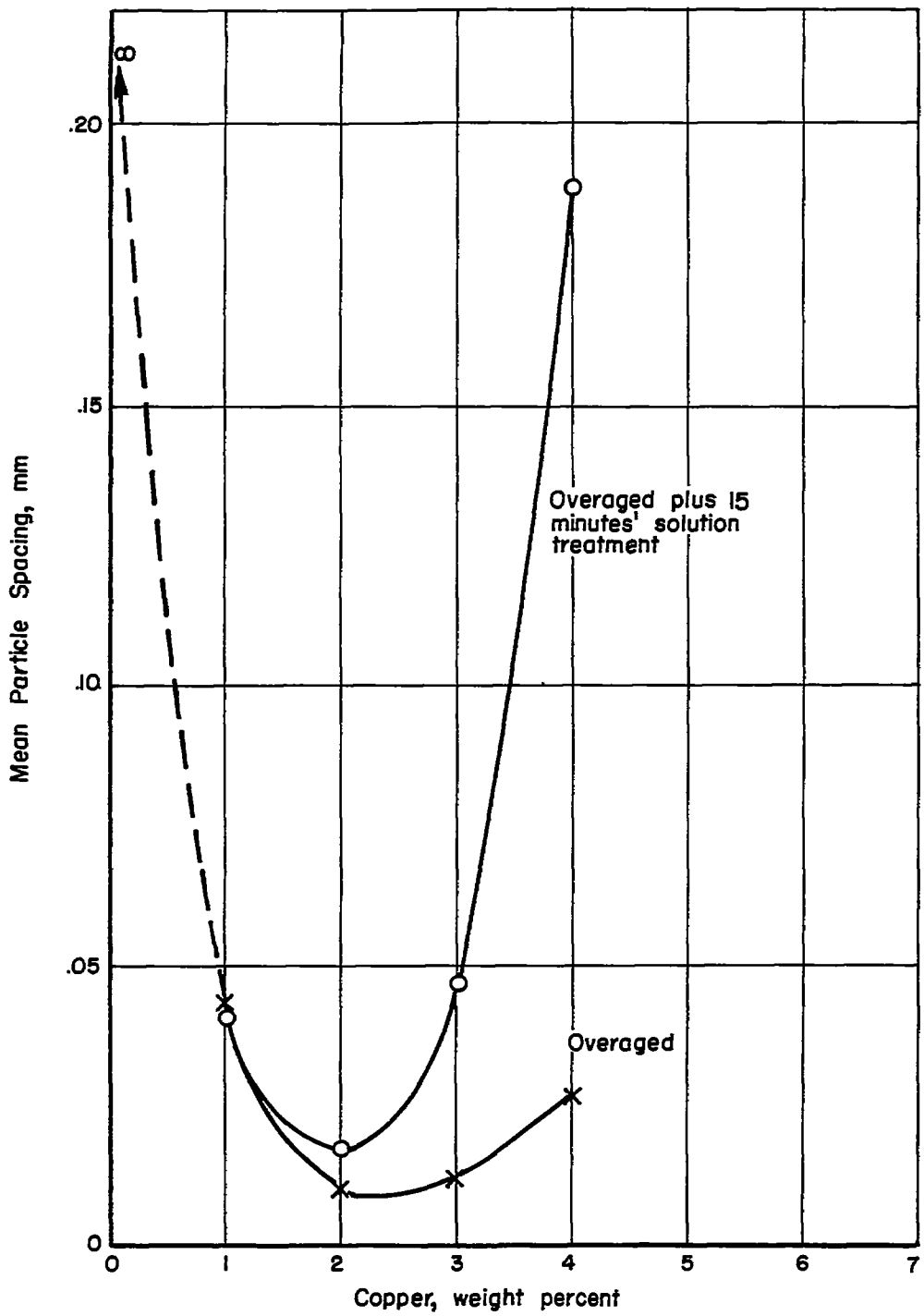

Figure 9.- Change in mean particle spacing of overaged aluminum-copper alloys after solution treatment.

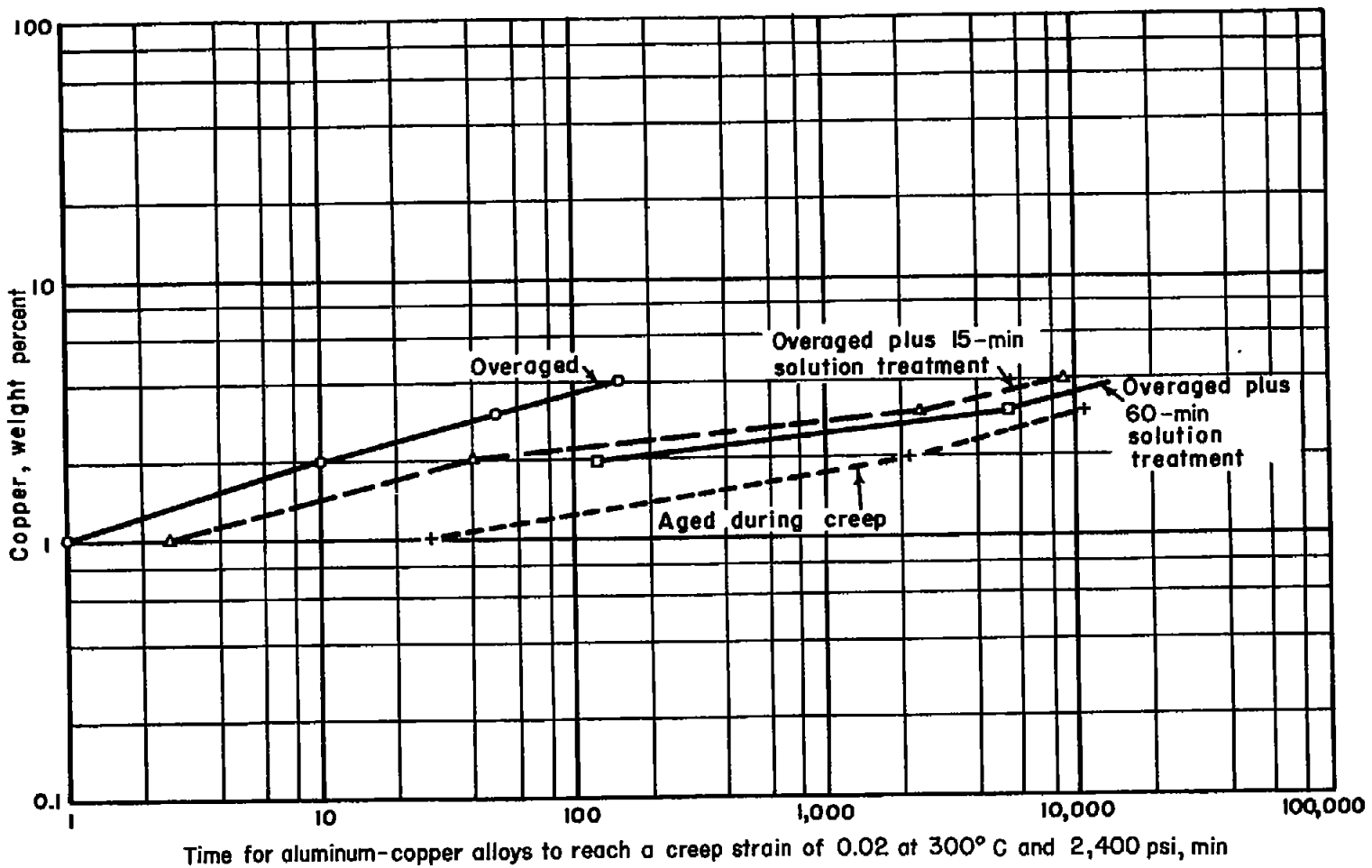

Figure 10.- Change in creep resistance of aluminum-copper alloys with different initial structures.

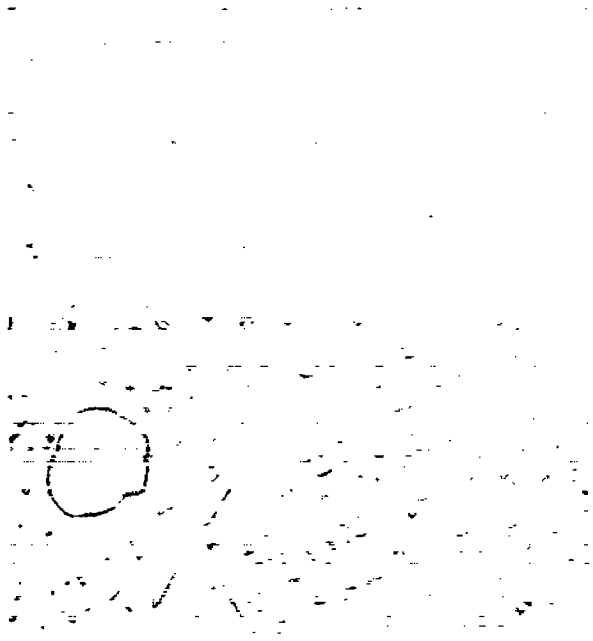

(a) Specimen 4-1-15T; X250.

(b) Specimen 4-1-15T; X1,500.

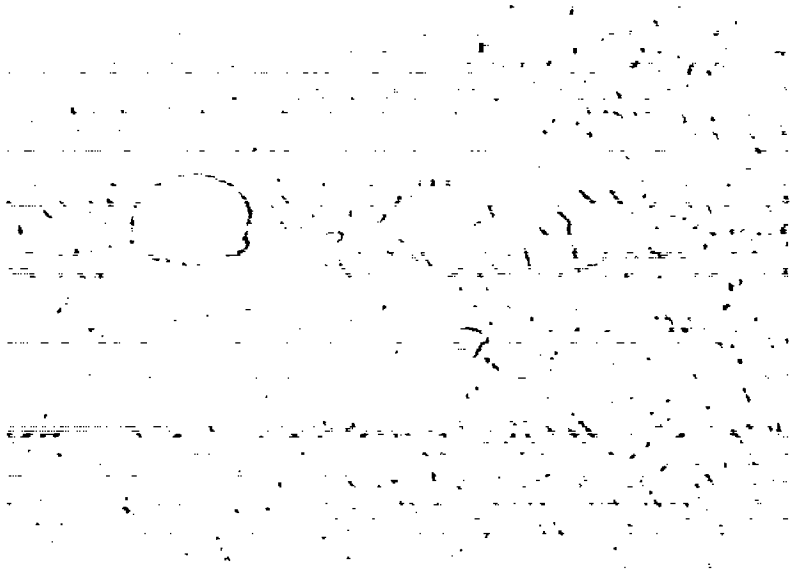

(c) Specimen 4-1-5S; X1,500.

Figure 11.- Stress-induced precipitate in aluminum alloys containing 4 percent copper and creep-tested at 300° C under 2,800 psi; Keller's etch. Initial condition was heavily overaged to large spherical particles.

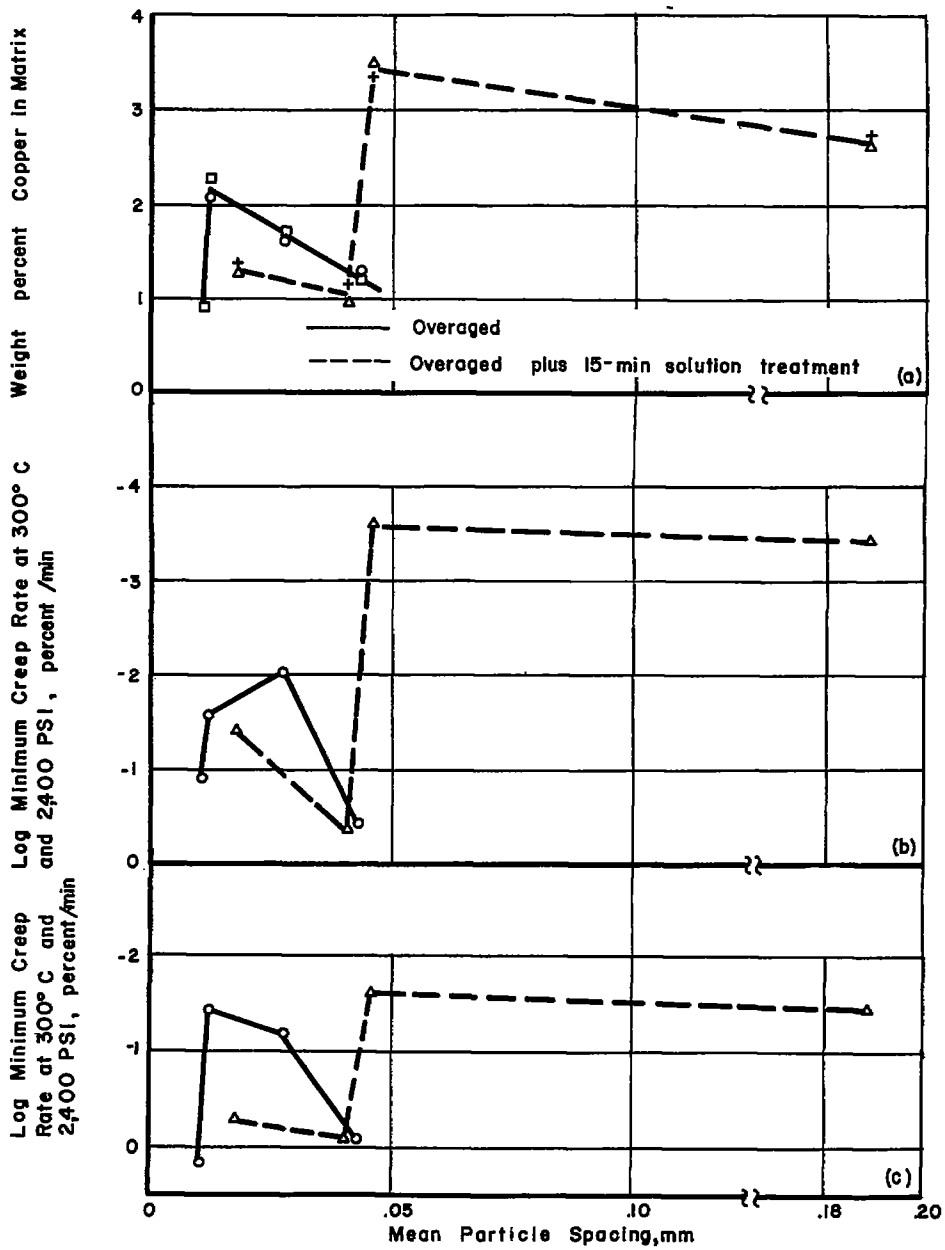

(a) Weight percent copper in matrix versus mean particle spacing.

(b) Measured values for particulate alloys.

(c) Calculated values for matrix of alloys.

Figure 12.- Compositions and minimum creep rates for aluminum-copper alloys with spherical precipitate θ.

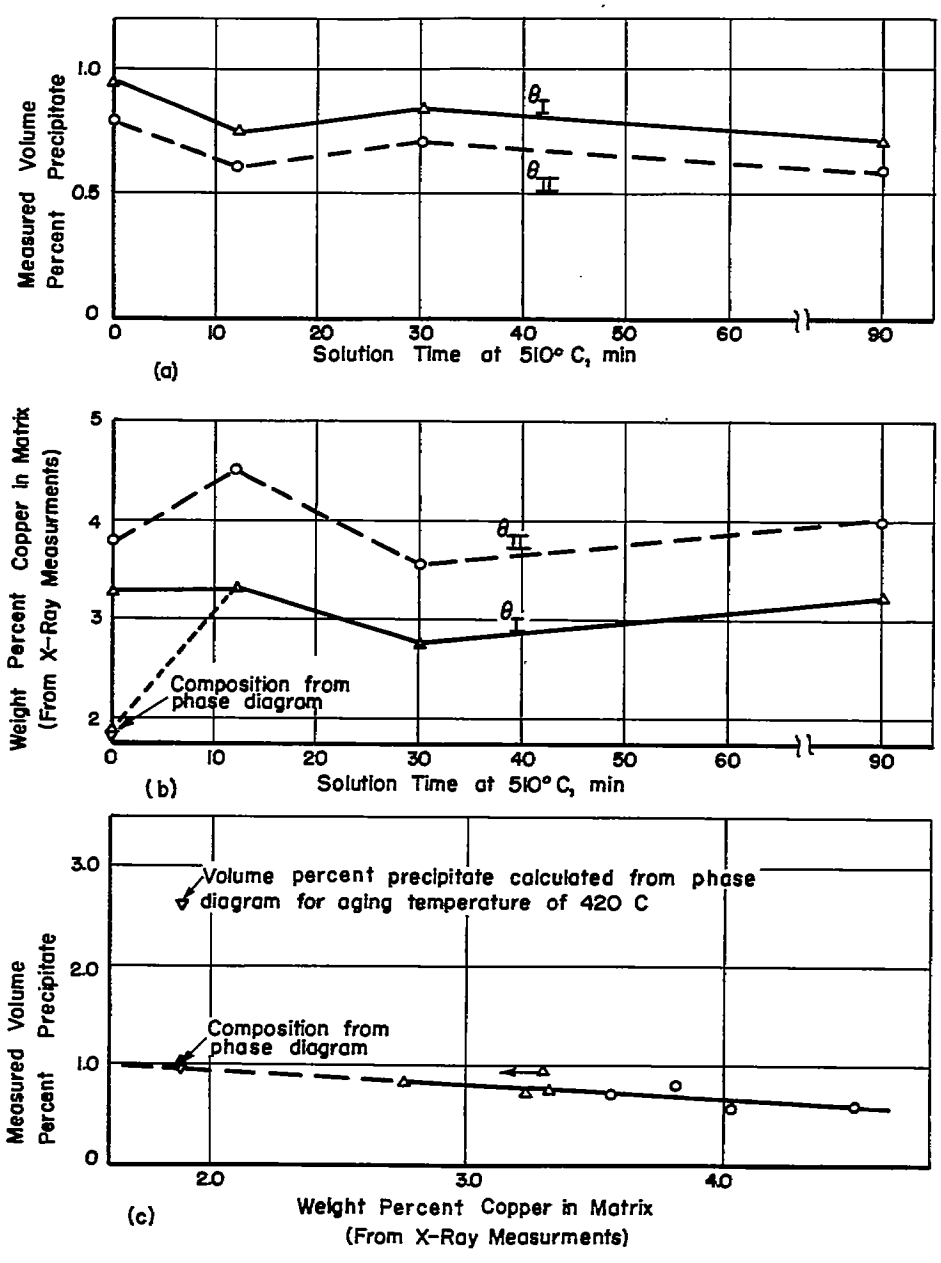

(a) Solution time versus measured volume.

(b) Solution time versus weight percent copper.

(c) Weight percent copper versus measured volume.

Figure 13.- Volume percent precipitate and matrix compositions for aluminum-copper alloys with spherical precipitate θ_I and θ_{II}.

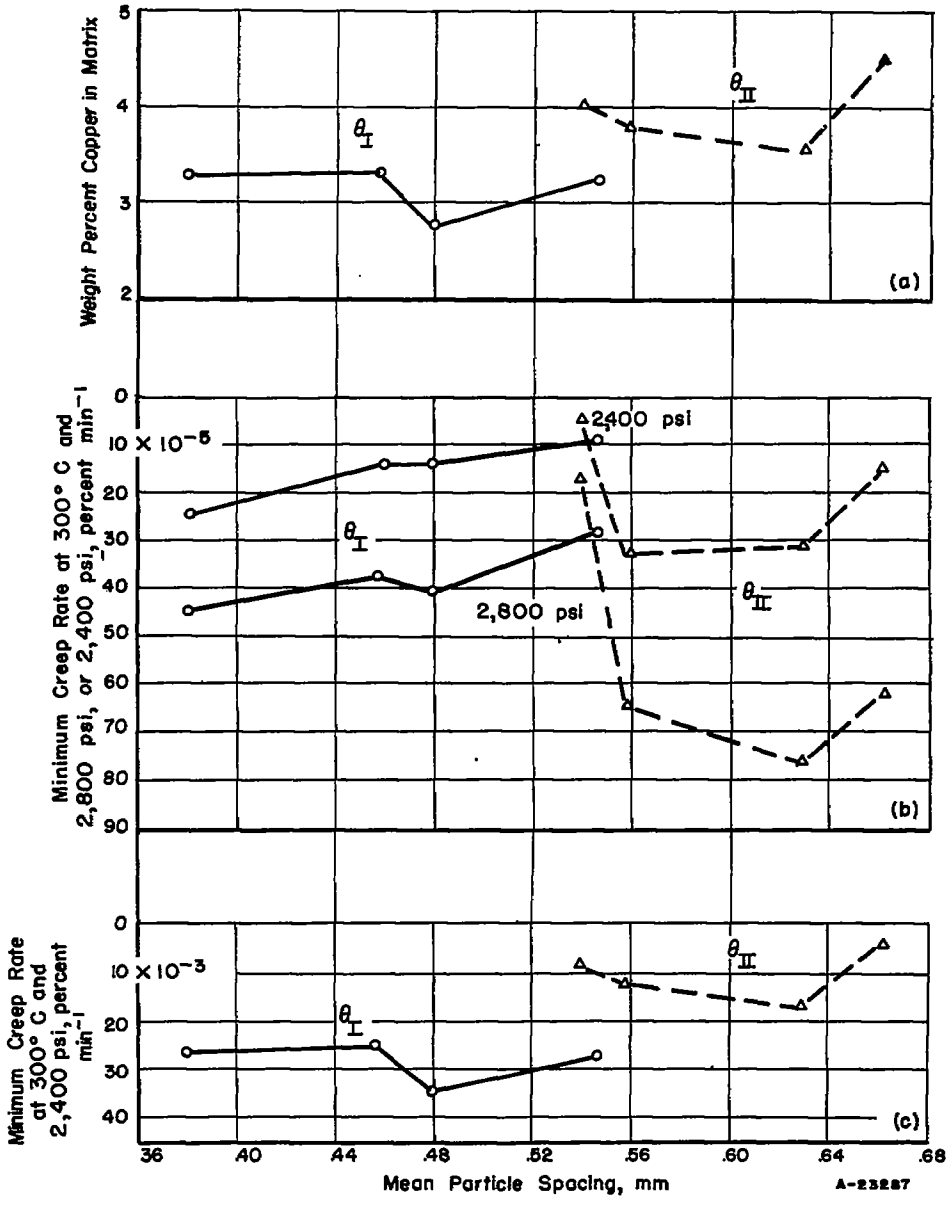

(a) Weight percent copper versus mean particle spacing.

(b) Measured values for particulate alloy.

(c) Calculated values for matrix of alloy.

Figure 14.- Compositions and minimum creep rates for aluminum-copper alloys with spherical precipitate θ_I and θ_{II}.

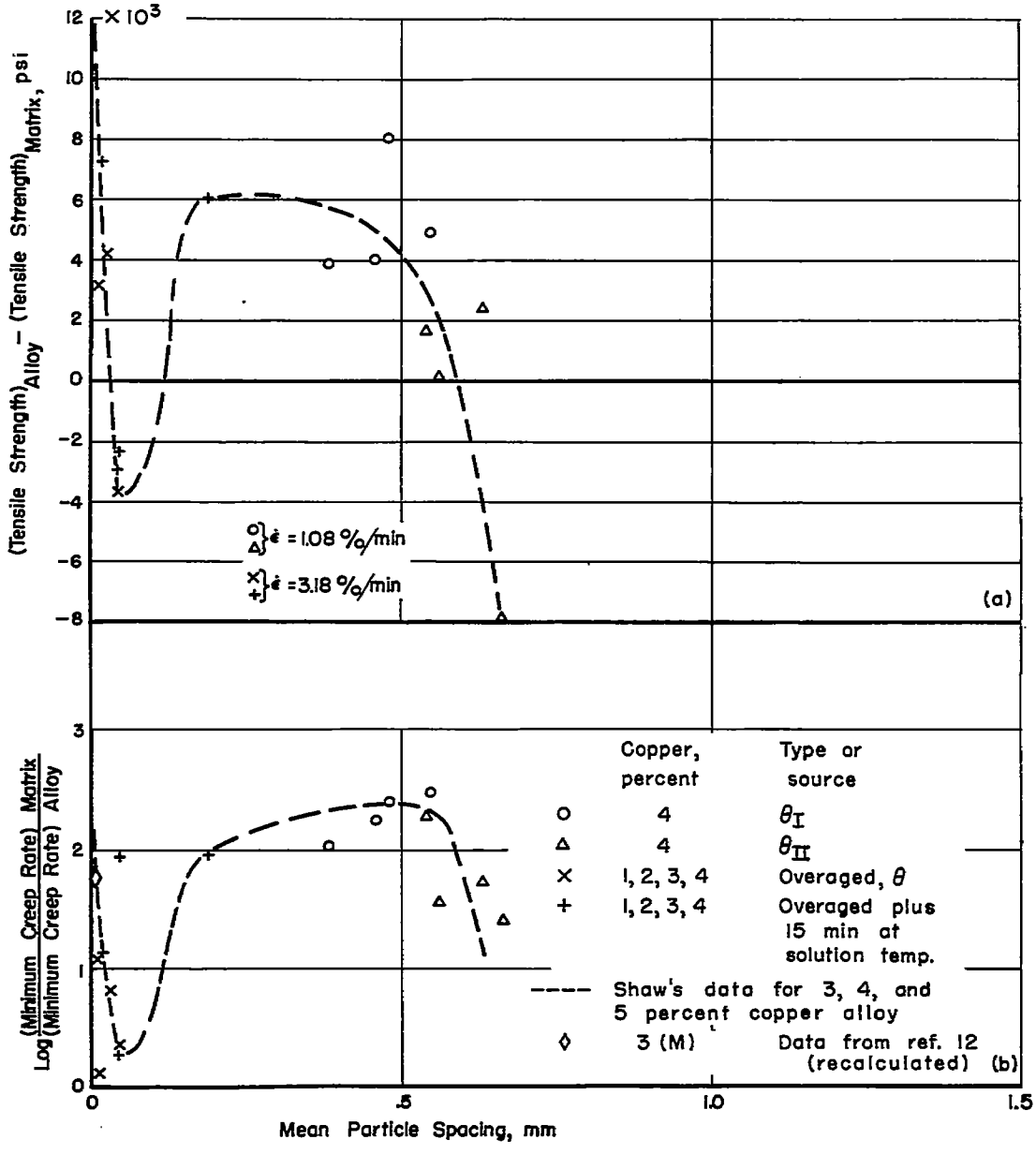

(a) Tensile data obtained at room temperature.

(b) Creep data obtained at 300° C under 2,400 psi.

Figure 15.- Increase in tensile strength and creep strength of aluminum-copper alloys over that of alloy matrix versus mean spacing of spherical particles. Matrix compositions derived from uncorrected X-ray lattice parameters.

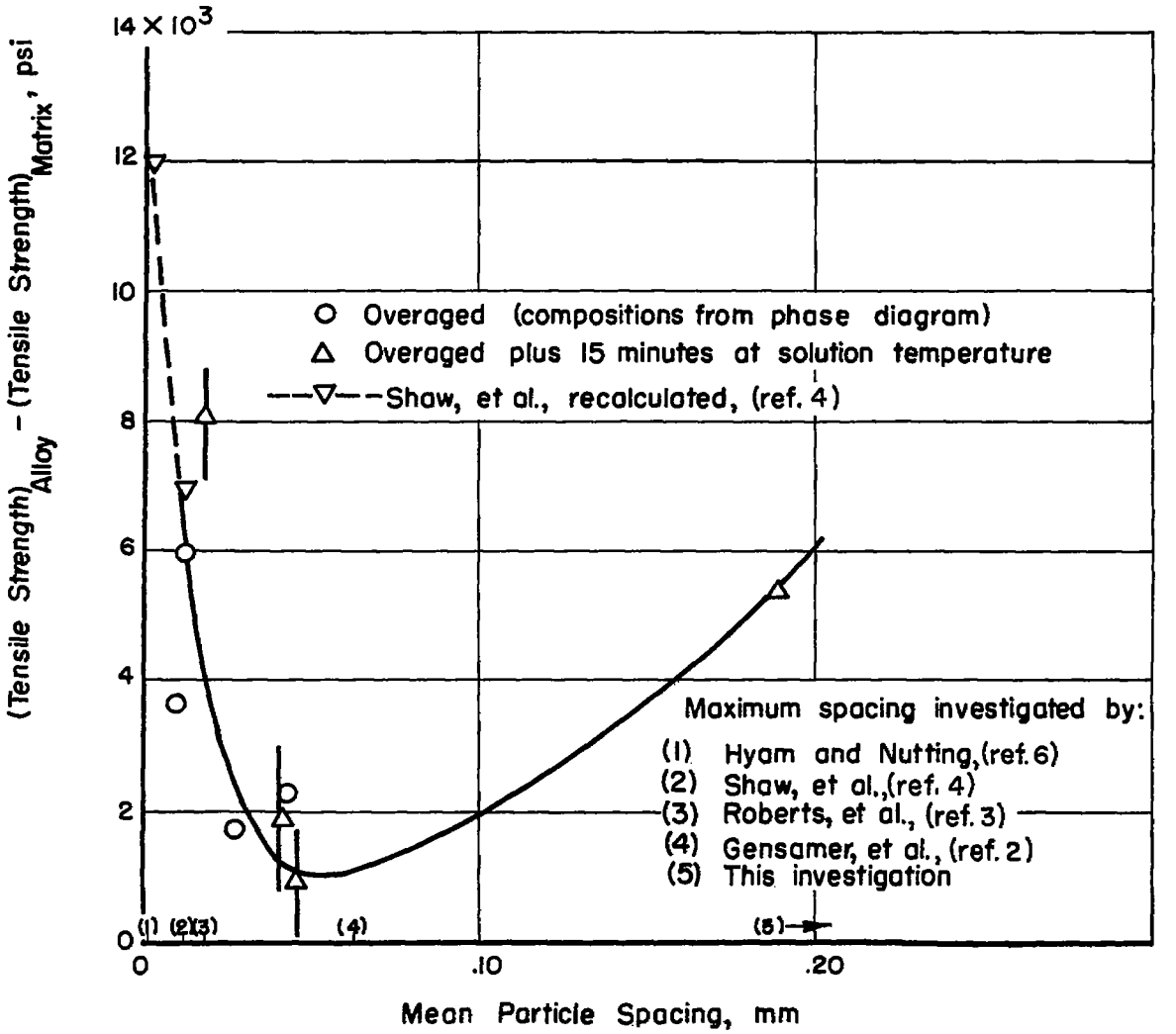

Figure 16.- Increase in room-temperature tensile strength of aluminum-copper alloys over that of alloy matrix versus mean spacing of spherical particles θ.

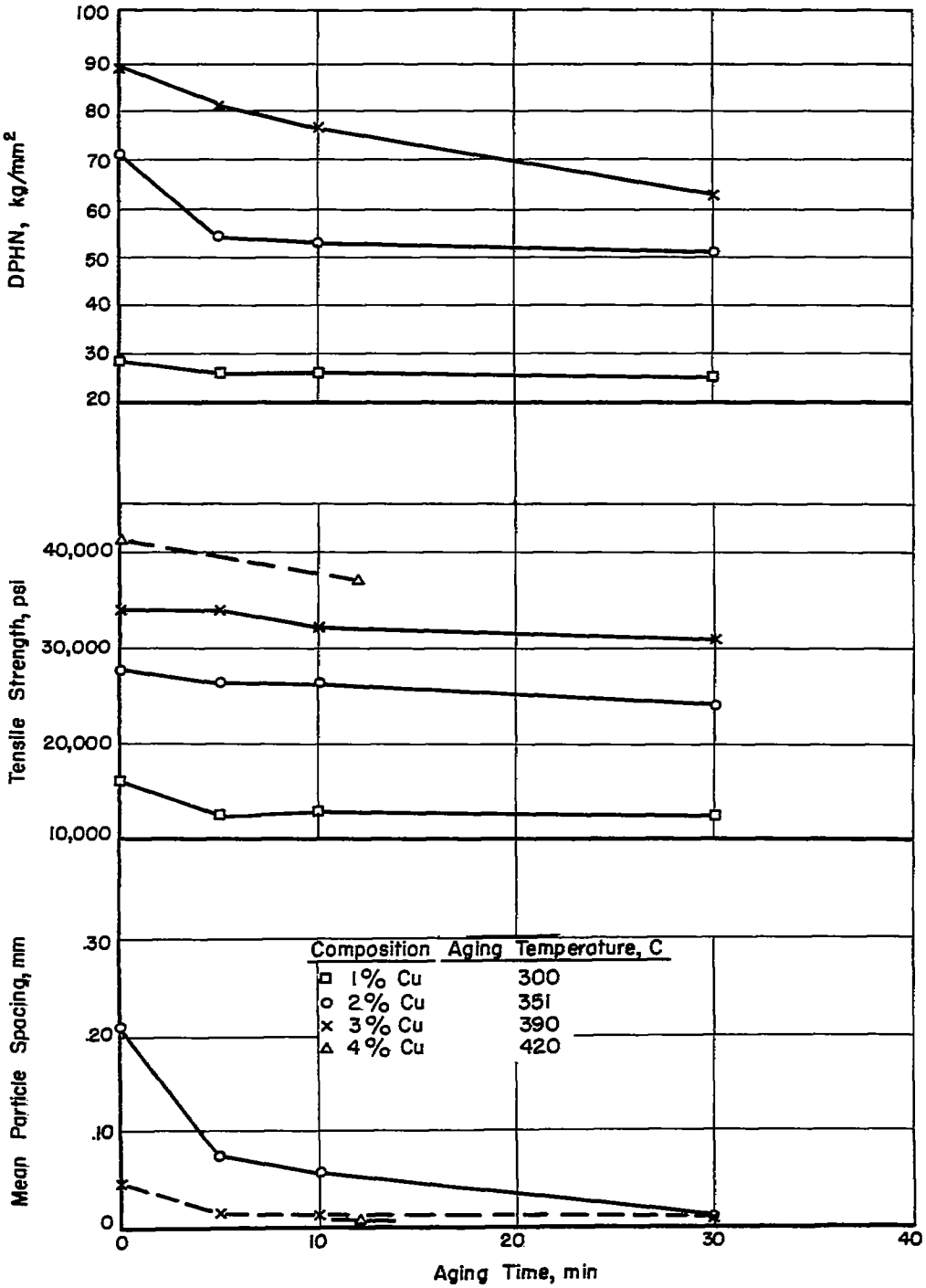

Figure 17.- Room-temperature properties of single-phase aluminum-copper alloys aged for various times to produce θ' structures.

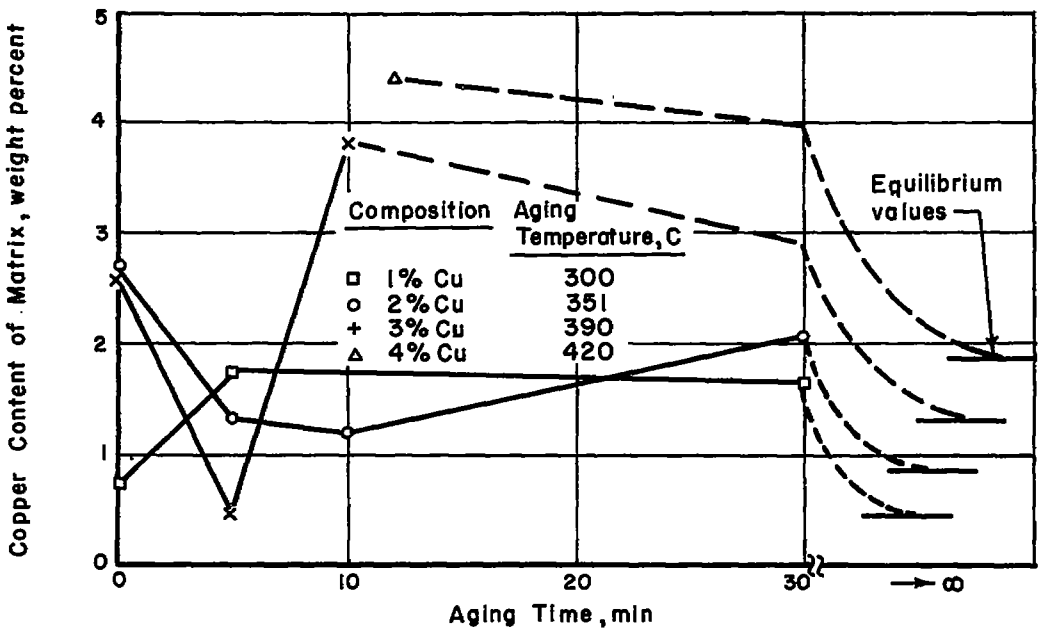

(a) Percent copper content versus aging time.

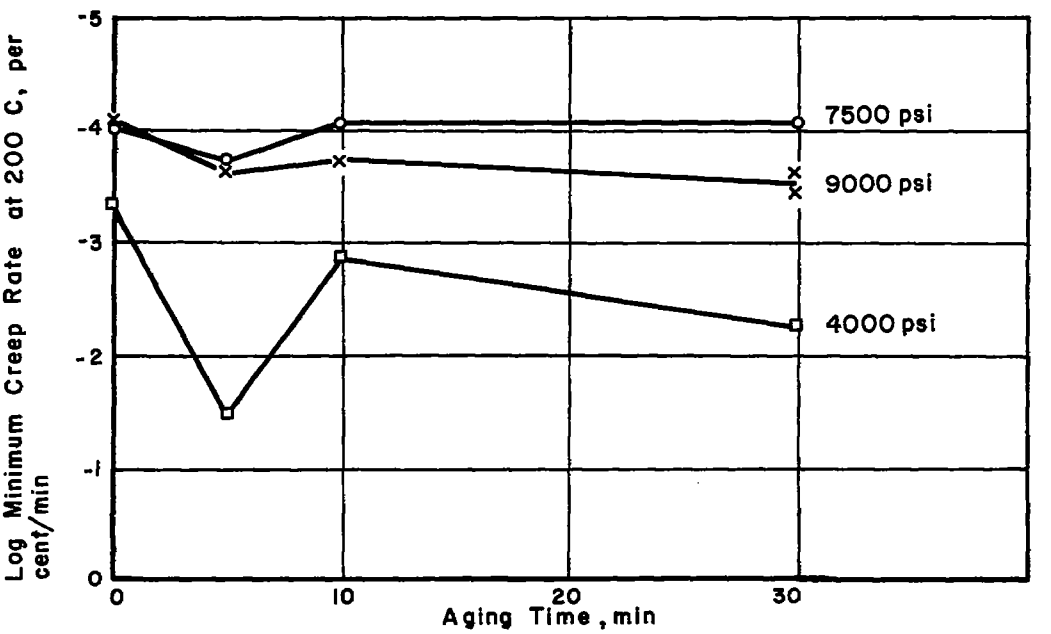

(b) Minimum creep rate versus aging time.

Figure 18.- Matrix of θ' alloys creep-tested at 200° C.

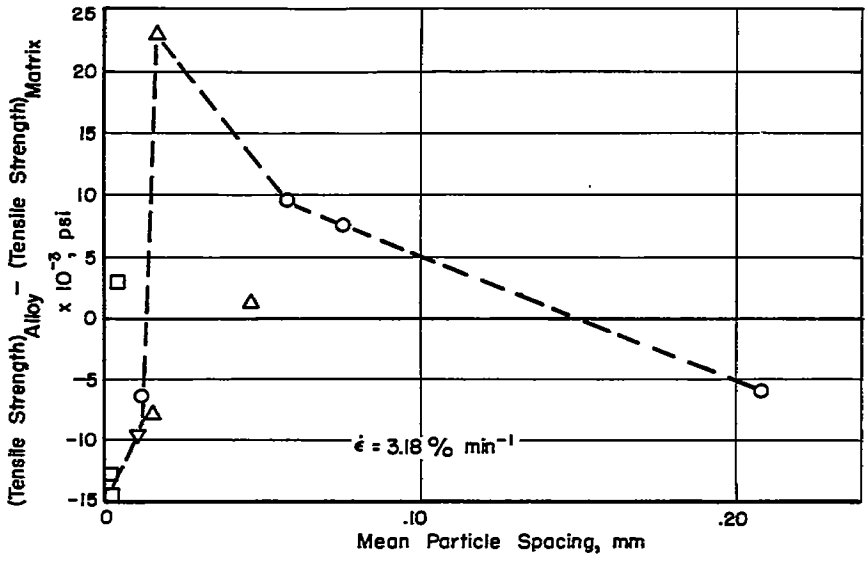

(a) Creep data at 200° C under 6,000 psi.

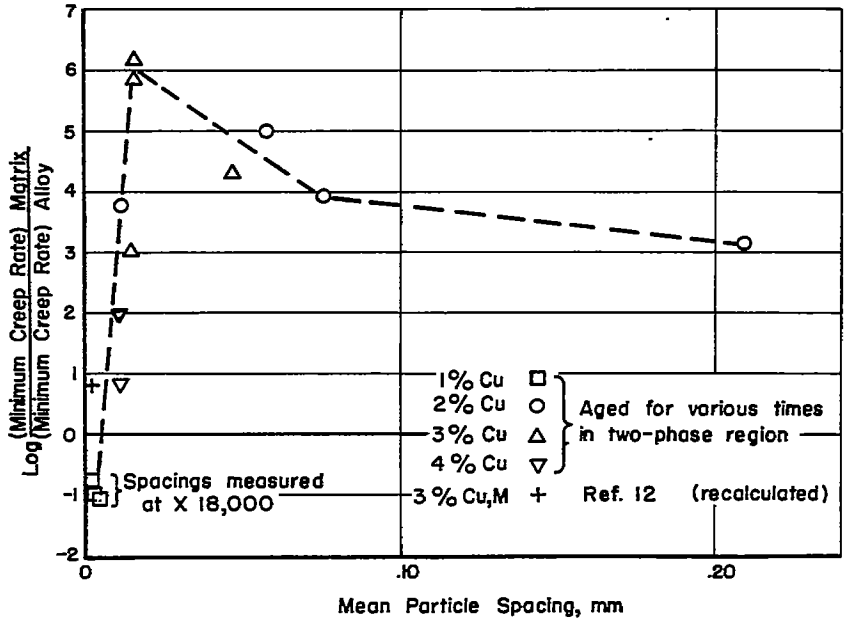

(b) Tensile data taken at room temperature.

Figure 19.- Increase in tensile strength and creep strength of aluminum-copper alloy over that of alloy matrix versus mean spacing of plate-like particles θ'. Matrix compositions derived from uncorrected X-ray lattice parameters.

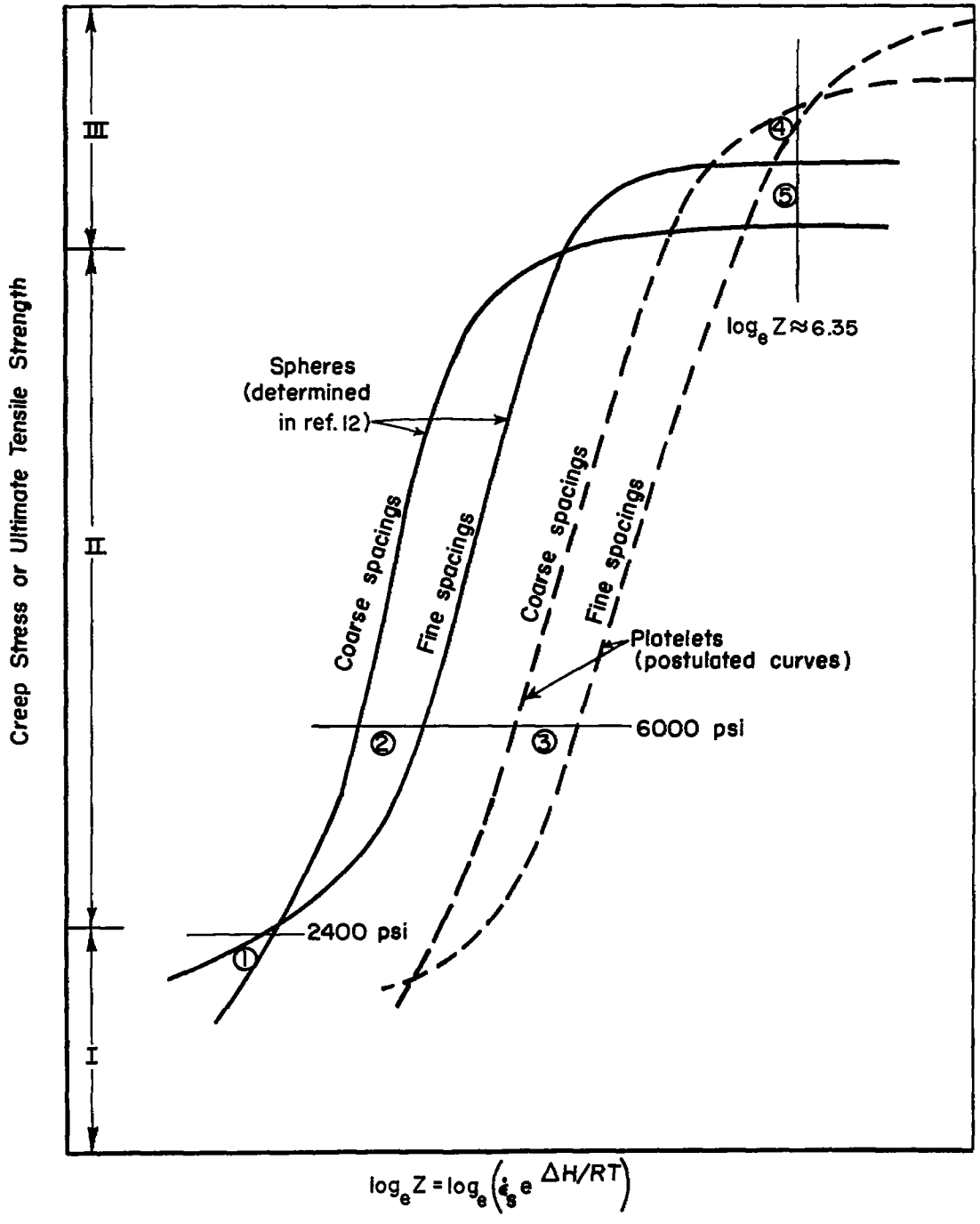

Figure 20.- Comparison of strength curves for alloys with platelets with those for alloys with spherical particles. For discussion of locations (1) to (5) see text, page 21.